REPORT

Earth Sciences and Environmental Technologies Division

Study	MPN12	**Division chrono**	*RXXX/n° YY-XXXX*
Partners	*NGI, KIGAM*	**Contract**	1997C0022

Title	**Assuring integrity of CO2 storage sites through ground surface monitoring (SENSE) – WP3.2: Application of inversion technique to onshore and offshore data (Deliverable D3.2)**		
Author(s) and membership	BOUQUET Sarah, FREY Jeremy, MALINOUSKAYA Iryna		
Diffusion	Confidential	**Publication date**	*m/d/yyyy*
Division visa *Scientific authentication*	ROGGERO Frédéric	**Project visa** *Specification compliance*	ROGGERO Frédéric

Keywords	Underground CO2 storage – CCS – Surface displacement – Monitoring – Coupled flow-geomechanical simulation – In Salah – Inversion – History-Matching – Dual-Medium – InSAR data - Fractures

Summary

The SENSE project is funded through the ACT program (Accelerating CCS Technologies, Horizon2020 Project No 294766). Its objective is to demonstrate how surface displacements can be used in a monitoring program aimed at verifying the long-term integrity of a CO_2 geological storage site. IFPEN participates as WP2 (Work Package) leader to coordinate 3D coupled hydromechanical simulation activities to understand the surface displacement mechanism in response to pressure changes due to CO_2 injection and contributes to the history-matching effort of WP3. This report addresses the Task 3.2: Application of inversion techniques to onshore and offshore data.

In our study, the application case is an onshore CO_2 injection site: the In Salah CO_2 storage project. This work relies on an existing In Salah model, updated for conformity with the coupled hydromechanical simulator presented in deliverable 2.3, calibrated with injection data and compared to processed InSAR data in WP1 from NGI (Norwegian Geotechnical Institute, partner of SENSE project).

Rich text

Earth Sciences and Environmental Technologies Division

Diffusion list (pdf)	E-mail address
HUYGHE Raphael	
SOUQUE Christine	
ESNAULT Vivien	
GERVAIS-COUPLET Véronique	
VINCKE Olivier	
ESTUBLIER Audrey	
ALAVOINE Axelle	
BOHLOLI Bahman (NGI)	Bahman.Bohloli@ngi.no
TOMA Oksana (ADEME)	oksana.toma@ademe.fr
CACAS-STENTZ Marie-Christine	
DOUARCHE Frédéric	
FREY Jérémy	
ROGGERO Frédéric	

For agreement,

Table of contents

1 Introduction

The In Salah site is a good candidate to study the effects of CO_2 injection on surface displacement and the potential of Interferometric Synthetic Aperture Radar (InSAR) surface monitoring. Carbon dioxide has been injected in the Krechba field in Algeria between August 2004 and June 2011. The surface of the storage site has been monitored through InSAR technology during and after injection. Surface displacements of several mm/yr were observed. A 3D seismic survey was also performed during this project. An unexpected behavior has been encountered while injecting CO_2 with a CO_2 migration through a legacy well (KB-5), another injected CO_2 breakthrough at a production well (KB-14) and a specific surface displacement footprint at one injection well (KB-502) described as a double-lobe deformation. This could be explained by a damaged zone that would allow a vertical migration of fluid through the caprock. According to White et al., 2013, this damaged zone could be a hydro-fractured zone triggered by the injection or an area of preexisting fractures (permeable or reactivated by the injection). In addition, the In Salah storage formation has a low-permeable matrix but a fractured medium. Based on previous studies (Deflandre et al., 2011), the modelling of a dual porous medium is required to be able to reproduce the storage behavior. Finally, several injection wells analyses demonstrate that fracture pressure was reached at the injection wells (*e.g.,* Bohloli et al. 2018; Shi et al., 2019), enhancing locally permeability and leading to a dynamic permeability definition for several models of In Salah (*e.g.,* Rinaldi et al., 2017; Bjornara et al., 2018; Shi et al., 2019).
The purpose of this report is to apply the new dual medium coupling scheme described in Deliverable 2.3 to the In Salah case and to compare results with pressure field data and InSAR data newly processed by SENSE partner (NGI). At first, a field description is supplied with the main elements to constrain the In Salah modelling. A brief review of previous In Salah modelling work is also performed. Then, the current In Salah modelling is described with the dual-medium scheme. Finally, history-matching results and more general comparisons with field data are presented.

2 In Salah project context and literature review

2.1 In Salah gas project

The In Salah gas development project was initiated in 2004. It is a large multi-field development (eight gas fields, including the Krechba reservoir) with 5 - 10% CO_2 in gas reservoirs (Figure 1). Rather than venting the extracted CO_2 into the atmosphere, operators chose to compress, dehydrate, transport, and inject CO_2 into a deep saline aquifer leg of the Krechba gas reservoir.

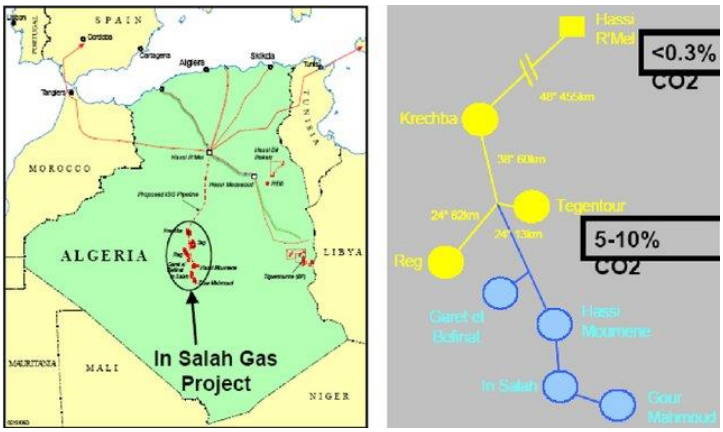

Figure 1 : After Himri et al. 2013, In Salah gas project situation.

Natural gas is produced at Krechba field with five horizontal production wells (Kb-11, 12, 13, 14 & 15). CO_2 was injected through three horizontal injection wells at 1500-1800m depth (Kb-501, 502, 503) (Figure 2). To maximize the injectivity, wells are oriented perpendicular to the direction of maximum stress, the dominant fracture direction (Vasco et al. 2018). The long-term plan was to store up to 17 million tonnes of carbon dioxide during the life of the program (Mathieson et al. 2010). However, about 3.8 Mt of CO_2 have been stored in approximately 7 years (Bohloli et al. 2018). Injection started in August 2004 and stopped definitively in June 2011.

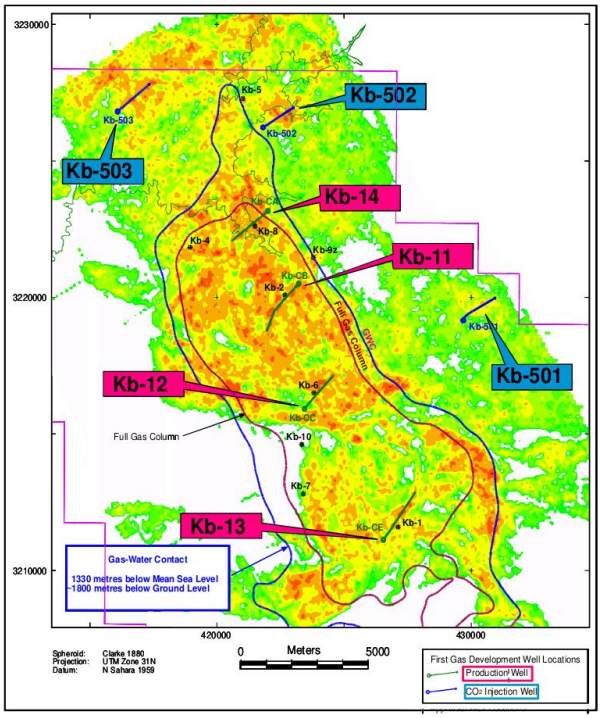

Figure 2 : From Baroni et al., 2011. Seismic porosity map at Krechba field with well locations and gas-water contact at 1330 m ss.

2.2 In Salah site specificities

The Krechba field has a gentle anticline structure that lies above reactivated basement faults and was influenced by strike-slip faults propagating up from the underlying Devonian formations (Ringrose et al., 2009). The anticline hosted a significant volume of gas (production well area), meaning that the mudstone seal is an effective caprock, preventing flow out of the reservoir.

One specificity of the Krechba site is that the target storage formation is a fractured-influenced, matrix-dominated sandstone formation (Ringrose et al., 2009). This formation has a relatively small storage volume in terms of overall reservoir thickness (20m-thick) and low average porosities (from 10 to 18%). It is a thin Carboniferous sandstone formation (C10.2, Figure 3) with a low matrix permeability (~10 mD). However, permeability measurements vary between 0.1 and 300mD due to variable cementation. Storage volume and reservoir permeability should likely be increased with fractures, but detailed/quantified effect of existing fractures was not known prior to the injection.

Above the storage formation is another 20m-thick tight sandstone formation, that can be considered as a secondary storage formation. The seal of the storage interval is a 950m-thick of Carboniferous Visean mudstones. The seal is overlain by an additional 900 m, the Continental Intracalaire sandstone that forms the regional Pan Saharan potable aquifer, a major source of fresh water.

The storage conditions are 90°C and 175 bar at 1800 m depth, meaning that CO_2 is supercritical in the storage formation.

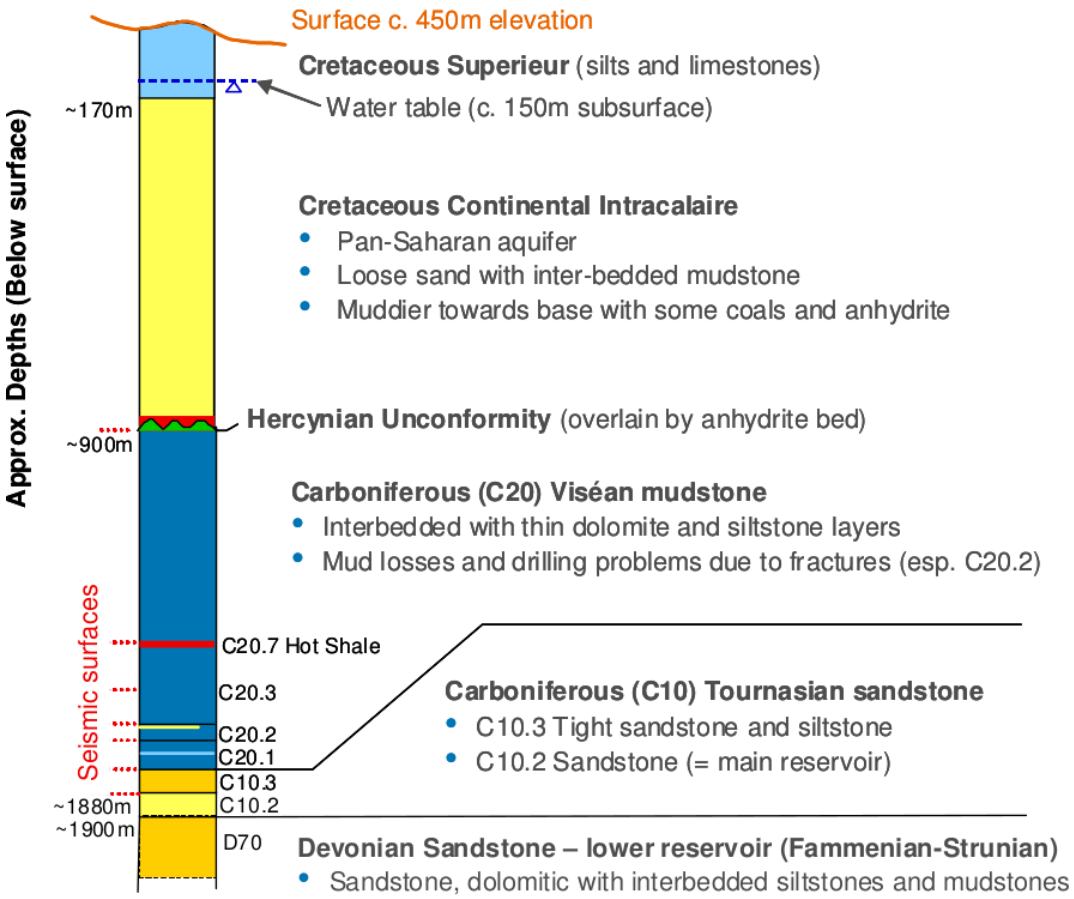

Figure 3 : From Deflandre et al., 2011. Krechba stratigraphic units.

2.3 In Salah site characterization

Part of the characterization comes from well data (Iding and Ringrose, 2010; Bissel et al., 2011; Vasco et al., 2018) thanks to the production history:

- Good well-logs suite (17 wells)
- Cores from C10.2 and C10.3 units (7 wells) with evidence of cemented fracture being conductive at surface conditions (Figure 4, Iding and Ringrose, 2010). Core observations are consistent with image log data and dynamic flow response (mud losses). Near-vertical conductive fractures do influence reservoir permeability. Fractures are also present in the overlying tight C10.2 sandstone unit. Cores are also used for porosity-permeability measurements.
- Mud losses data and Image logs from KB14 (Formation Micro-Imager, FMI in C20.3 interval) and KB-502 (FMI in C20.1 to C20.2) and CBI (C10.2 reservoir) (Iding and Ringrose, 2010):
    - Injection horizon (C10.2) & immediate overburden (C20) are naturally fractured with a northwesterly fracture orientation
    - C10 : 1-5 NW fractures / m, aperture 0.1 – 1 mm & lengths 50 – 200 m
    - C20 : 1-3 NW fractures / m, aperture 0.1 - 1 mm & lengths 50 – 200 m

  These data have been used to build several DFN (Discrete Fracture Network) models to infer the fracture permeability in different direction at two wells (Iding and Ringrose, 2010). Lateral permeability varies between 150 and 400 md while vertical permeability varies between 400 and 1000 mD.

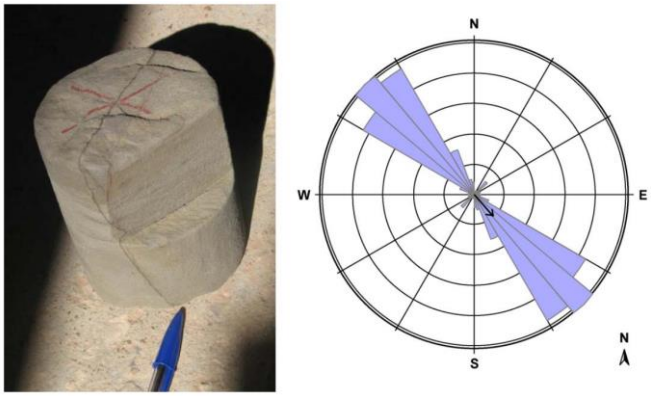

Figure 4 : From Iding and Ringrose, 2010. Fracture data: Partially cemented fracture in core sample from well KB-2 (left), Rose diagram with fractures orientation obtained from FMI and UBI image logs in well KB-502z (right).

- Gas sampling (isotubes) from wells KB-14 and KB-502
- Rock mechanical studies (core and log based). Tests are performed on several samples to measure unconfined compressive strength (UCS), Young's modulus (E) and Poisson's ratio (PR) in the direction perpendicular to the bedding. Logs give range of values for those mechanical properties function of depth. UCS, UTS values can be used to calculate friction and cohesion (based on Drucker-Prager criterion definition). Geomechanical reference dataset is given in Table 1.

Table 1 : Reproduced from Ringrose et al. (2017). Geomechanical reference dataset for the In Salah site.

Geological Unit	Young's Modulus, E (GPa)	Poisson's ratio, ν	Depth interval, MD (m)	Comments
Shallow Aquifer (Cretaceous)	3	0.25	0-885	Very uncertain
Main Caprock (Visean)	5	0.3	885-1635	Very uncertain
Lower Caprock (Visean)	2	0.3	1635-1747	Very uncertain
Tight sandstone (C10.3) (Carboniferous)	20	0.25	1747-1763	Good log data
Reservoir (C10.2) (Carboniferous)	10	0.2	1763-1782	Good log data
Underburden (Devonian)	15	0.3	Below base	Good log data

- Stress Estimation:
  - The stress regime is a strike-slip regime:
    - the largest principal stress in the horizontal NW-SE direction (315/135 degrees)
    - the intermediate principal stress is oriented vertically
    - the least principal stress is in the NE-SW direction
  - The vertical stress σ_v is determined by integrating a density log extending from the surface to a depth of a few hundred meters above the reservoir (1650 m) at KB-502. The estimate obtained is 44.5 MPa in reservoir (Morris et al. 2011). This would be equivalent to a value obtained using a constant density of 2.283 g/cc (Vasco et al., 2018).
  - Leak-off tests (LOF) and formation integrity tests (FIT) are used to infer the minimum horizontal principal stress estimates. Large uncertainties remain since estimates are not from actual stress measurements (Vasco et al., 2018). The minimum horizontal stress in reservoir is 30.8 MPa according to Morris et al. (2011) but 29.5 MPa for Shi et al. (2019).
  - The maximum horizontal stress is estimated with wellbore failure data from image and caliper logs (assuming to have the same depth trend as the vertical stress) at 49.9 MPa in reservoir (Morris et al. 2011).
    - Above 1620m (1170m TVD): $\sigma_H / \sigma_v = 1.09$
    - Below 1620m (1170m TVD): $\sigma_H / \sigma_v = 1.12$

Estimates of fracture pressure were mainly performed based on well test interpretation and are described in the monitoring section.

The In Salah site was also characterized through two seismic surveys.
The first one is a regional seismic survey in 1997, thus before the injection (Figure 5). Based on these seismic data, no major faults have been detected in the overburden/caprock, neither in the injection formation, but minor faulting (close to the limit of seismic detection) can be observed in the Carboniferous and lower overburden (Mathieson et al., 2010). This would be due to deep seated faults in the Devonian underburden, propagating in the Carboniferous level (section flexed over the Devonian) and may control the minor faults and NW-SE fractures in the CO_2 storage formation. The second seismic survey was performed during the injection period and is described in the next section.

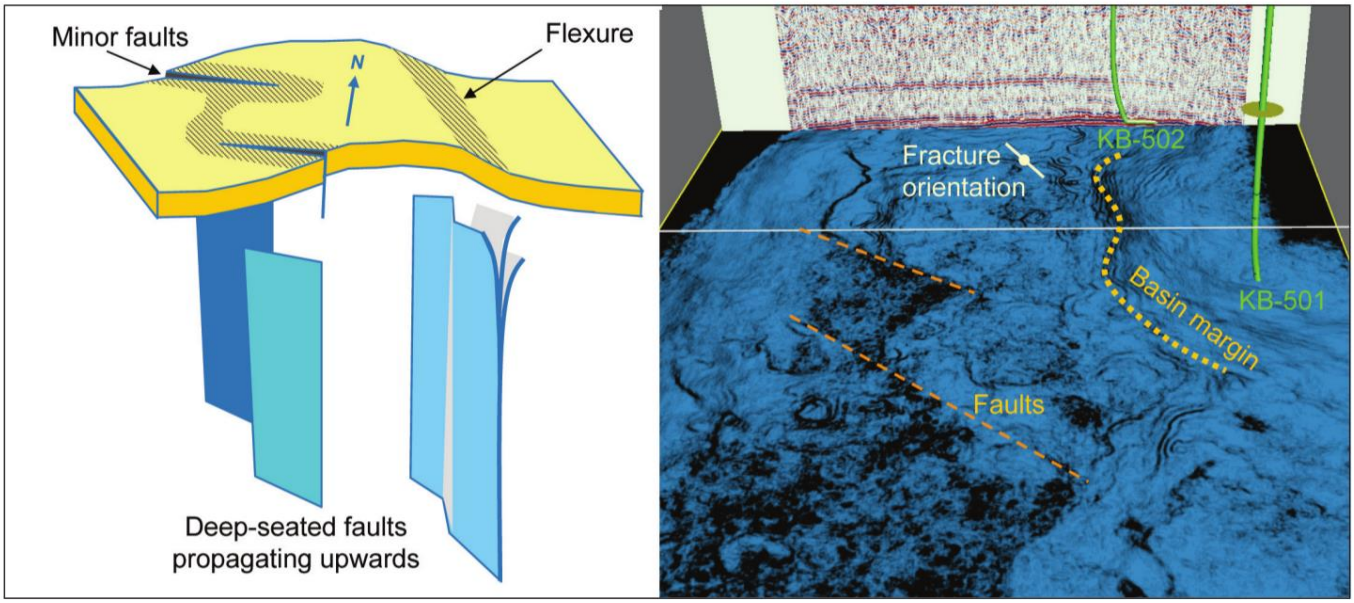

Figure 5 : From Ringrose et al. 2009. Structural geological setting (left) inferred from seismic data at reservoir level (right, 1997 regional seismic survey).

2.4 In Salah injection monitoring

An extensive monitoring plan was considered for the In Salah site (see Figure 6, table from Mathieson et al., 2010 summarizing the monitoring techniques). According to Vasco et al., 2018, the most important data for this CO_2 storage monitoring came from well pressure and fluid sampling, InSAR data, 3D seismic and micro-seismic monitoring. It should be noticed that tiltmeters data were never available and micro-seismic detection was significantly delayed but collected data coincides with estimates fracture pressure. In the following, we will focus on wells, InSAR and 3D seismic data.

Monitoring technology	Risk to monitor	Action
Wellhead/annulus sampling	Wellbore integrity Plume migration	• Twice-monthly sampling since 2005
Tracers	Plume migration	• Implemented 2006
Wireline logging/sampling	Subsurface characterization	• Overburden samples and logs collected in new development wells
Soil gas/surface flux	Surface seepage	• Preinjection surveys in 2004 • Repeat survey in 2009
3D-4D seismic	Plume migration	• Initial survey in 1997 • High-resolution survey acquired in mid-2009. Provides feasibility evaluation for 4D
Deep-observation wells	Plume migration	• Not planned at present due to cost
Microseismic	Cap rock integrity	• Test well drilled mid-2009 above KB-502 injector • Depth 500 m, 1500 m above injection zone, 50 geophones array (10 three-component) • Recording ongoing
Electromagnetic surface and wellbore	Plume migration	• Not useful at Krechba due to subsurface architecture and logistics • Wells too widely spaced
Gravity	Plume migration	• Modeling suggests surface response negligible • May be tested in 2011 • Borehole gravity possible if suitable access available
VSP	Cap rock integrity Plume migration Fracture evaluation	• Modeling results inconclusive • Decision pending 3D VSP into microseismic array
Shallow aquifer wells	Contamination of potable aquifer Cap rock breach	• Seven shallow aquifer wells drilled • Sampling twice per year
Microbiology	Surface seepage	• First samples collected in late 2009
Eddy covariance flux towers and LIDARs	Surface seepage	• Reviewed, but weather conditions and potential equipment theft ruled this out • Reviewing potential for deployment in 2011
InSAR monitoring	Plume migration Cap rock integrity Pressure development	• Used extensively, contributions and commissioned work from several providers • Images captured every 28 days
Tiltmeters/GPS	Plume migration Cap rock integrity Pressure development	• To calibrate InSAR deformations • 70 tiltmeters deployed around KB-501 in late 2009

Figure 6 : From Mathieson et al. 2010, Monitoring technologies considered at In Salah site.

2.4.1 Well pressure and fluid sampling

Based on WellHead pressures (WHP), temperatures and flow rates, fracture pressures were estimated for each injection well. The estimate for KB-502 is around 28.6 MPa from Bissel et al. (2011) but could be lowered by 1.5 to 5 MPa due to cooling effect of relatively cold CO_2 injection. Shi et al. (2012) and White et al. (2014) give an estimate around 30 MPa while Shi et al. (2019) re-estimate the fracture pressure of KB-502 at 28.5 MPa (Figure 7). Based on WHP measurement, Bohloli et al. (2018) estimate the fracture WHP at 15.5 MPa, equivalent to about 27.7 MPa for the BHP (Bottom-Hole Pressure). The estimates for KB-501 are about 17.8 MPa in term of WHP (Bohloli et al., 2018), 32.5 MPa in term of BHP from Shi et al. (2019) but 29.0 MPa from a Leak-Off Test according to Bissel et al. (2011). The estimates for KB-503 are 17.5 MPa in term of WHP (Bohloli et al., 2018) and 31.0 MPa in term of BHP (Shi et al., 2019).

One should notice that all estimates in term of BHP values are uncertain because BHP are inferred from WHP, temperature, and flow rates. No bottom data are available; thus, no calibration on BHP or error estimates can be performed.

Nevertheless, beyond the exact fracture pressure estimate, it is clearly observed that all three wells' BHPs went beyond the formation fracture pressure (Figure 7).

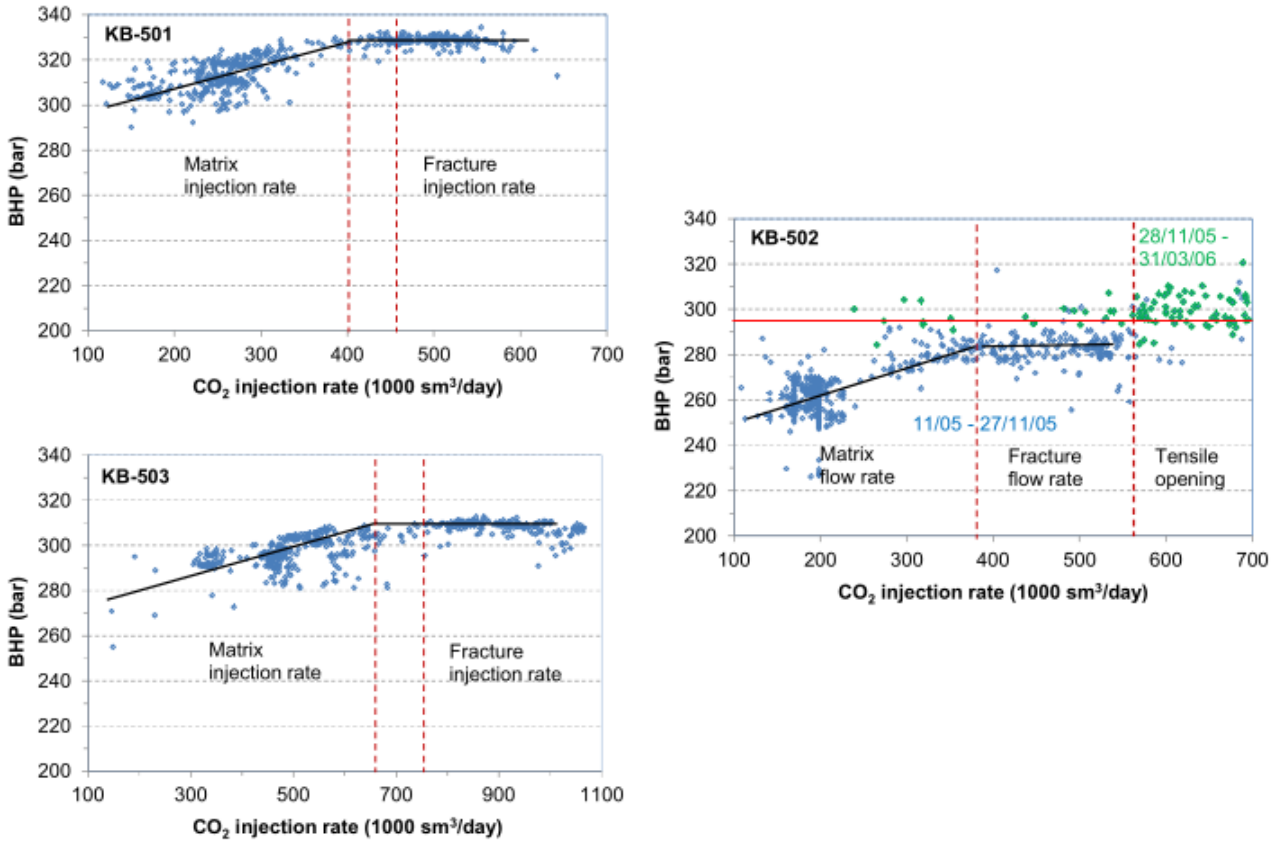

Figure 7: From Shi et al. 2019. Injection pressure versus injection rate for wells KB-501 and KB-503 between March and July 2008; for well KB-502 between May 2005 and March 2006. The red line represents the estimated minimum horizontal stress (295 bars). Before fracturing, pressure clearly increases with the increase in injection rate. When fracturing, the slope changes, with almost a constant pressure while still increasing the injection rate.

Between August 2006 and June 2007, a CO_2 breakthrough was detected in the old KB-5 appraisal well (about one km north of KB-502). Tracers' analyses confirmed that the detected CO_2 came from KB-502 well (Mathieson et al., 2011). More efforts were performed on monitoring to understand and explain this CO_2 breakthrough via InSAR and seismic monitoring.
Another CO_2 breakthrough was detected 1-year post-injection (2012) at KB-14 well, a production well about 5 km from the injector KB-502. This arrival was predicted by Bissel's numerical simulation (Ringrose et al. 2013).

2.4.2 InSAR monitoring

InSAR monitoring is a satellite data acquisition technique which, after processing, can provide displacement maps covering at least the entire storage area. This method was successfully applied to In Salah storage site where surface displacement (uplift) related to CO_2 injection was monitored at all three injection wells (Figure 8). For the first few years of injection, the uplift is about 5mm/yr over each injection well (Vasco et al., 2018) with a maximum uplift between 20 and 25 mm.
From these observations, the particular double-lobe pattern above KB-502 well (Figures 8 and 9) was studied and commented by many authors (e.g., Vasco et al., 2010; Morris et al., 2011; Shi et al., 2012; Rinaldi and Rutqvist, 2013; White et al., 2014; Bjornara et al., 2018). This pattern would be explained by a vertical conductive zone (with time) in the lower caprock leading to the vertical fluid migration in this zone (Figure 10). The mechanisms involved in this dilation are not clearly identified but most probably would be due to the pressurization of an existing fracture zone or due to the hydrofracturing in this zone, related to the injection (White et al., 2014). This was supported by the latest 3D seismic survey in 2009, see next paragraph.

Some discussions were made about a potential existing fault (F12) between KB-502 and KB-5 from 1997 seismic survey but this was invalidated in 2009 seismic survey (of higher precision).

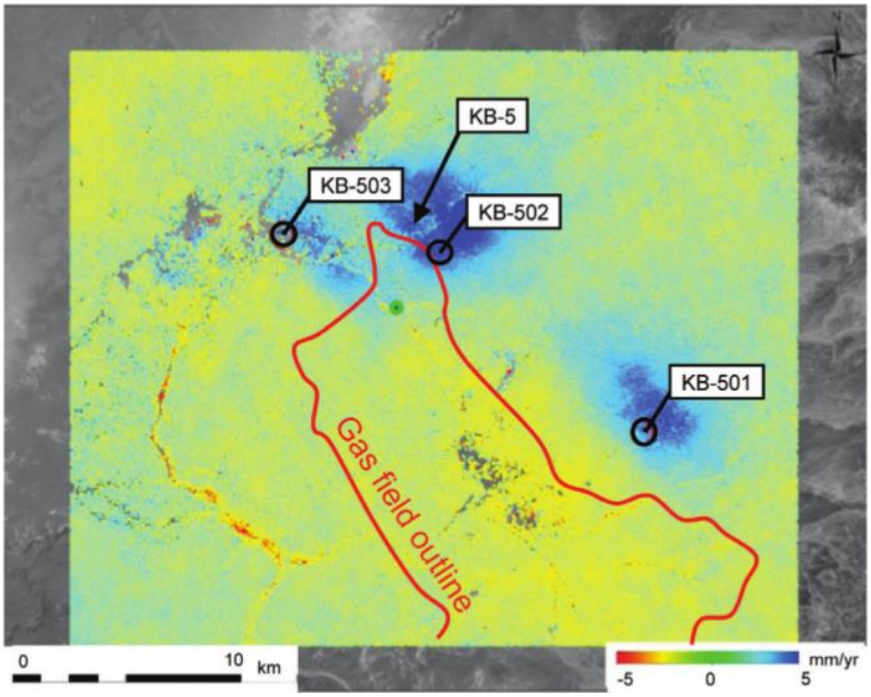

Figure 8: From Vasco et al. 2008, PSInSAR velocity map (Envisat) over the In Salah area between December 2003 and March 2007

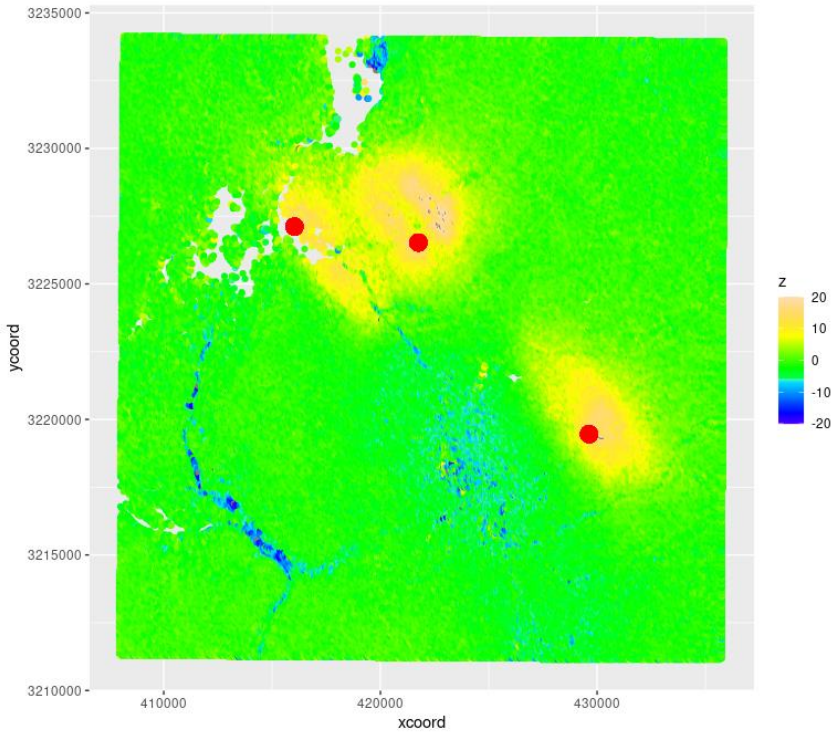

Figure 9 : Vertical displacement [mm] in February 2008 from re-processed InSAR data by NGI (SENSE, internal communication). Red dots are injection wells heads.

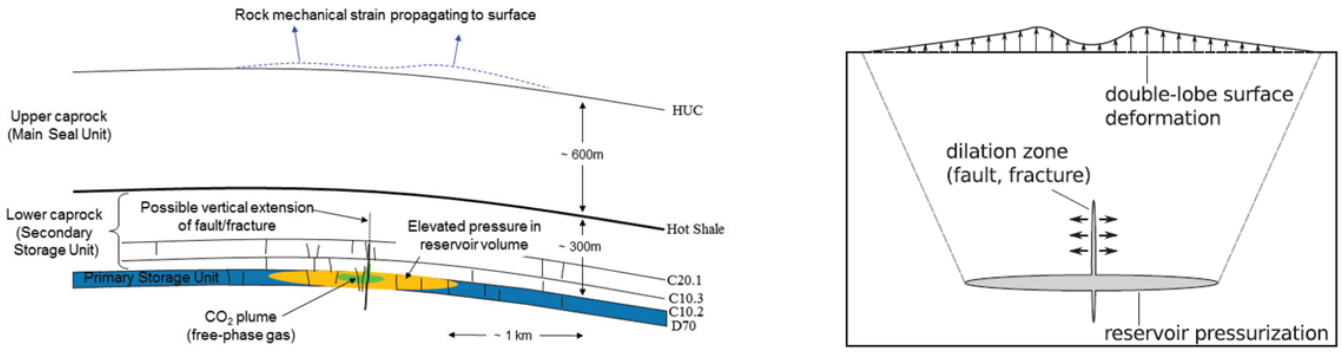

Figure 10 : Left: From Ringrose et al. (2013); Right: From White et al. (2014): Schematic illustration of the plausible deformation mechanism at the In Salah storage site.

2.4.3 Active 3D seismic survey

A 3D seismic survey was acquired in 2009, in a narrower area than in 1997 but with a much higher imaging quality. The deeper structures already observed in 1997, were verified by this 2009 seismic survey.
Regarding the two lobes observed in InSAR data at KB-502, some correspondence exists in seismic data with a sharp linear feature[1] located in between these lobes in few seismic horizons (Gibson-Poole and Raikes, 2010, see Figure 11). This would be due to the change in pressure and saturation related to the injection. This is interpreted as a fault, fracture, or damage zone, propagating from the reservoir up to the top of layer C20.4 (amplitude of the push down decreases at this top according to Vasco et al., 2018, from Zhang et all., 2015), allowing the vertical fluid migration. Zhang et al. (2015) estimate that the damage zone is approximately 3500 m long, 80 m wide, and 350 m high (Figure 12).

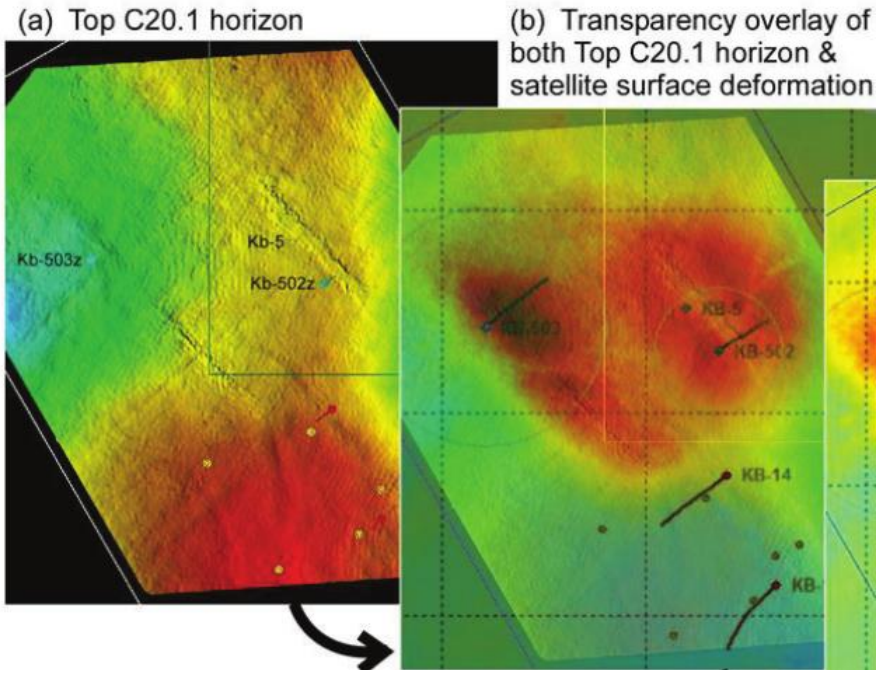

Figure 11 :From Vaso et al., 2018. Comparison between seismic time horizon (top C 20.1 horizon, i.e., lower caprock) and InSAR surface uplift data: coincidence in between sharp linear seismic feature and the separation between lobes: both sources give elements towards an upward CO_2 migration into the lower caprock.

[1] A similar linear feature was also observed to intersect well KB-503 and to extend several kilometers to the southeast (White et al. 2014).

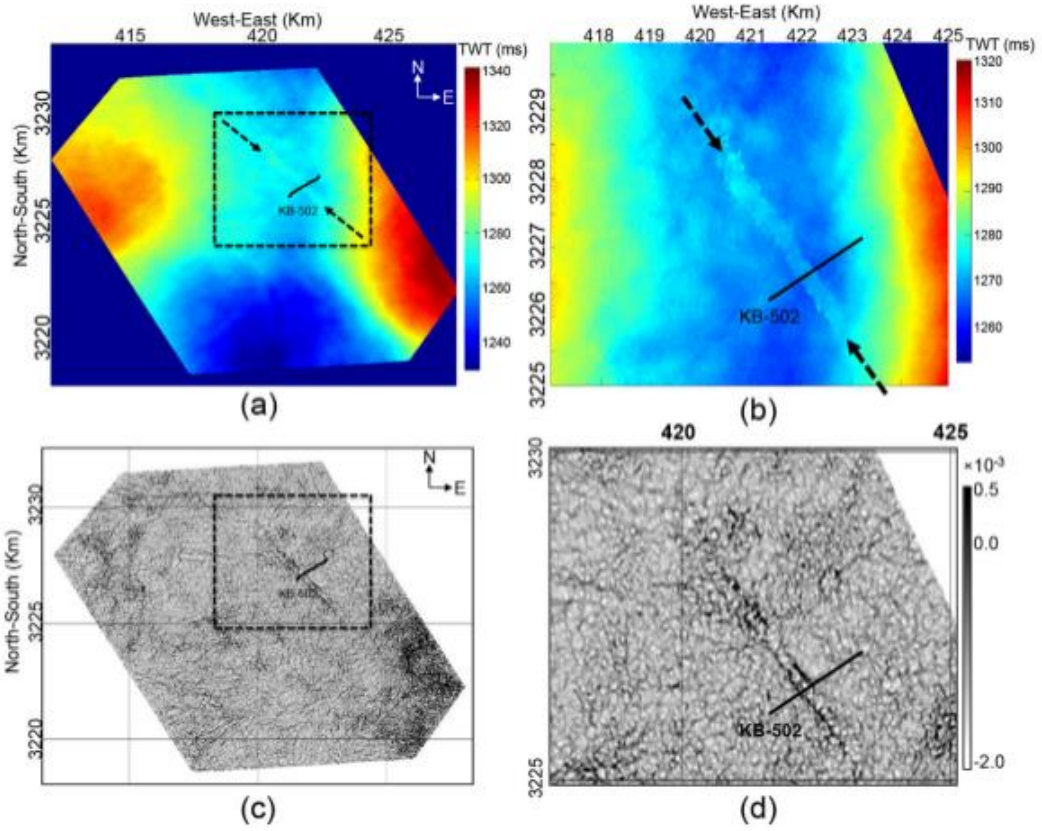

Fig. 4. (a) Shows mapped surface at the bottom of the overlain shale, and (b) shows the zoomed view within the black dashed rectangle of (a). (c) Shows the most positive curvature along the same surface, and (d) shows the zoomed view within the black dashed rectangle in (c).

Figure 12 : From Zhang et al., 2019: new seismic feature from the 2009 seismic survey in KB-502 area. This is aligned with InSAR results, see figure above.

2.5 In Salah – Existing models

CO_2 injection at the In Salah site has been subject to many modelling studies.

A first, conceptual model was performed by Vasco et al. 2010, to reproduce the specific displacement at KB-502 well with a fault/fracture zone 4-km long across this well trajectory and varying vertical elastic properties. Another conceptual modelling was realized by Rutqvist et al. (2010) to simulate surface displacement (InSAR data) at KB-501 and KB-503 through coupled hydromechanical model (TOUGH-FLAC). A detailed hydromechanical model (NUFT/SYNEF codes) of KB-502 well was studied by Morris et al. (2011) in order to match satellite data and gain in understanding in surface response to CO_2 injection at this location (sensitivity to overburden and "fault" properties).

A more comprehensive model of the In Salah site was simulated by Bissel et al. 2011, including a set of fractures around KB-502 well, heterogeneous flow properties, 3D constraints from seismic data and dynamic constraints from well BHPs as well as satellite data (commercial STARS/GEM simulator suite).

Another serie of models for the In Salah site was initiated as part of the CO2remove project with different kind of modellings: Deflandre et al. (2011), Baroni et al (2011) (Puma/Abaqus hydromechanical coupling) and Pamucku et al. (2011) (commercial Eclipse simulator) considered dual medium models and Shi et al (2012 and 2019) defined a permeable corridor across KB-502 well with varying transmissivity with time. The primary objective of these models was to history-match well pressure behavior and CO_2 breakthrough at KB-5 well.

Later studies from Bjornara et al.,2018 highlight the requirements of dynamic permeability (with pressure) to obtain a reasonable match of reservoir pressure and surface behavior. **Bissell et al. (2011), Shi et al. (2012, 2019), Bjornara et al. (2018), Rinaldi et al. (2013, 2017), all used a time-varying transmissivity to simulate the opening of the fracture and matched pressure.**

Except for dual medium models, the fault/fracture damage zone intersecting KB-502 has mostly been explicitly modelled through a permeable corridor into the reservoir and lower portion of the caprock.
Some examples of datasets for different In Salah modellings are given below in tables 2, 3, and 4.

Table 2 : Partial dataset from Baroni et al., 2011

Formation	Depth range, m	Young's modulus, GPa	Poisson's ratio	Permeability, md [mean]	Porosity [mean]
Shallow aquifer	0-900	3 - 3.3	0.25	1000	0.25
Caprock (C20)	900-1650	5	0.3	0.001	0.1
Lower caprock (C20.1-C20.3)	1650-1780	5 -7.7	0.2 - 0.3	0.001-0.1	0.05-0.10
Tight sandstone C10.3	1780-1800	7.2	0.09	0.02	0.01
Reservoir C10.2	1800-1820	8	0.17	1.9	0.18
Well Zone KB 501-502-503		8.4 - 3 - 18	0.1-0.16-0.17		
Underburden	1820-4000	10	0.3		

Table 3: Partial dataset from Bjornara et al., 2018

Formation	Depth range, m	Young's modulus, GPa	Poisson's ratio	Permeability, md	Porosity
Shallow aquifer	0-900	3	0.25		
Caprock (C20)	900-1650	5	0.3		
Lower caprock (C20.1-C20.3)	1650-1780	2	0.3		
Tight sandstone	1780-1800	20	0.25		
Reservoir C10.2	1800-1820	9	0.15	3 (initial but vary with pressure)	0.17
Fracture Zone	1870	0.4	0.15	3 (initial but vary with pressure)	0.2
Underburden	1820-4000	15	0.3		

Table 4 : Partial dataset from Rinaldi et al. (2013) for KB-502

Formation	Depth range, m	Young's modulus, GPa	Poisson ratio	Permeability, md	Porosity	Friction
Shallow aquifer	0-900	3	0.25	1000		
Caprock (C20)	900-1650	5	0.3	1e-6	0.1	
Lower caprock (C20.1-C20.3)	1650-1780	2	0.3	1e-6	0.1?	
Tight sandstone C10.3	1780-1800	20	0.25	1E-6	0.1	
Reservoir C10.2	1800-1820	10	0.2	80 (variable)	0.17	27.87
Fracture zone		x,y,z 0.17, 0.14, 1.0	0.25 [yz] 0.18[xy & xz]	100	0.01	30.55
Underburden	1820-4000	15	0.3	1e-4	0.01	

3 In Salah model setting and update

3.1 Previous IFPEN model setting

As explained in Deflandre et al. 2011, a reasonable history matching of pressure and KB-5 breakthrough time was obtained, using a dual-medium description of the In Salah site (dual porosity and dual permeability). This history-matching was performed for the first three and half years of the CO_2 injection project (from August 2004 to December 2007).

Porosity and permeability fields are heterogeneous in C10.2 and C10.3 formations (Figure 13). When performing the calibration, mean and standard deviation were modified. To match well data, the field was divided in four wells zones, as described in Baroni et al. (2011), resulting in different statistics in these different zones. For all parameters that are not detailed in the next section, we keep the same definition and value as in these two previous studies (Deflandre et al., 2011 and Baroni et al., 2011).

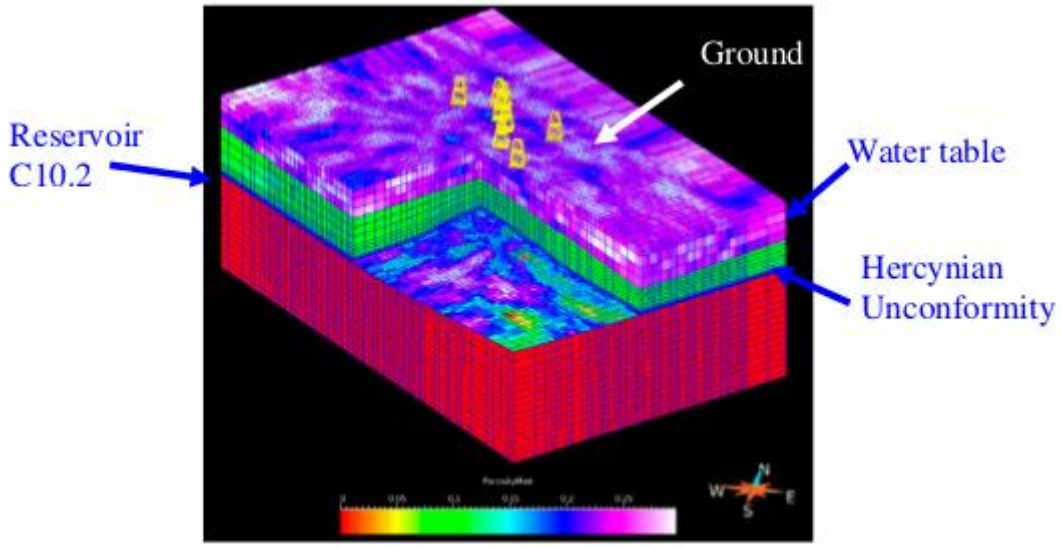

Figure 13 : From Deflandre et al. (2011), initial IFPEN model for Krechba field

3.2 Model updates

Previous mechanical calculations were performed with Abaqus (Baroni et al., 2011). In this study, we used the coupled hydromechanical calculations with PumaFlow and Code_Aster, described in Deliverables 2.2 (Bouquet et al., 2021) and modified for dual-medium model (Deliverable 2.3, Bouquet et al., 2022).

For compatibility with this hydromechanical coupling, the dataset and mesh were modified (stairsteps, model's thickness, flat bottom, *etc*.) (Figure 14).

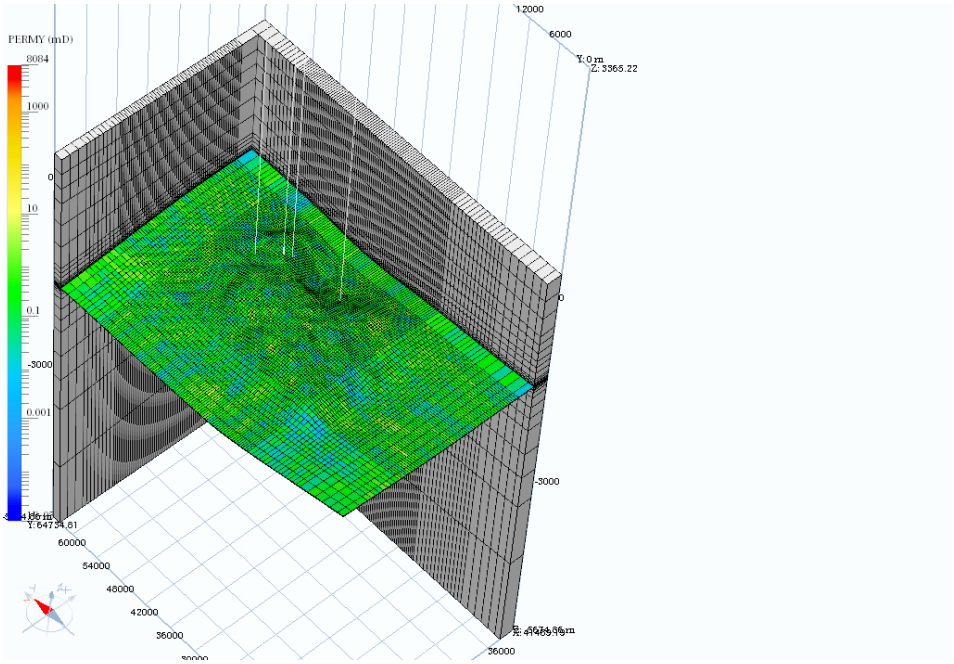

Figure 14 : 3D view of the updated In Salah model. Permeability field (K_Y) in C10.2 formation. White lines are KB501, KB5, KB502 and KB503 wells' locations.

The dual medium description is used for characterized fractured medium, *i.e.,* C10.3, C10.2 and Lower Caprock (C20.x) formations (Figure 15). Flow-activated layers for caprock and underburden are described only as a porous matrix medium. Inactive layers are flow-inactive. For mechanical simulation, all inactive layers have the same properties, but these properties are allowed to vary with depth.
To be able to simulate the stimulation or creation of a fracture zone, we keep the dual-porosity and dual-permeability formulation in C10.3, C10.2 and Lower Caprock formations. We use initial low porosity and permeability values in fractures in Lower Caprock. Thus, initially the fractures flow in Lower Caprock is negligible but porosity and permeability can be changed in time function of pressure results either through internal correlation from the flow simulator or more strictly with retroaction from the mechanical calculation on flow properties (iterative case).

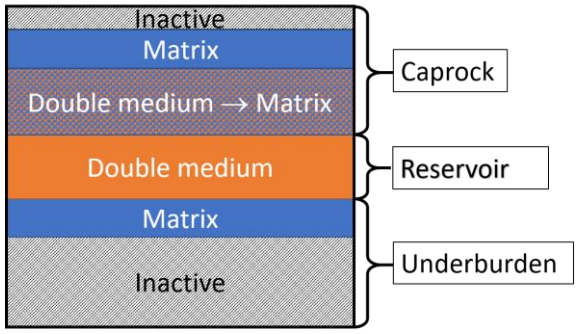

Figure 15 : Schematic view of the In Salah model

While a unique value of pore compressibility was applied for both fracture and matrix media and for all formations in the previous study, the new dataset includes different pore compressibility values per media (fracture and matrix) and for each formation. This to keep consistency between defined properties in flow and mechanical simulator, in particular for one-way simulations. Nevertheless, since porosity values vary spatially (i.e., variation in each cell) while we assign one value of pore compressibility per zone, the equivalent pore compressibility in flow simulation is not strictly consistent with mechanical properties (equivalent pore compressibility depends on porosity values). Moreover, because of uncertainties about the synthetic representation/model of the fracture

network (e.g., fracture shape, see Deliverable 2.3), the equivalent pore compressibility value remains at best a rough approximation.
Since the previous study, new injection data were made available and had to be added to this model. New wellheads data were shared from SENSE partner (KIGAM) from 2009 up to the beginning of 2011. Additionally, cumulative injection volume data were also shared and integrated in the new model (Figure 16).

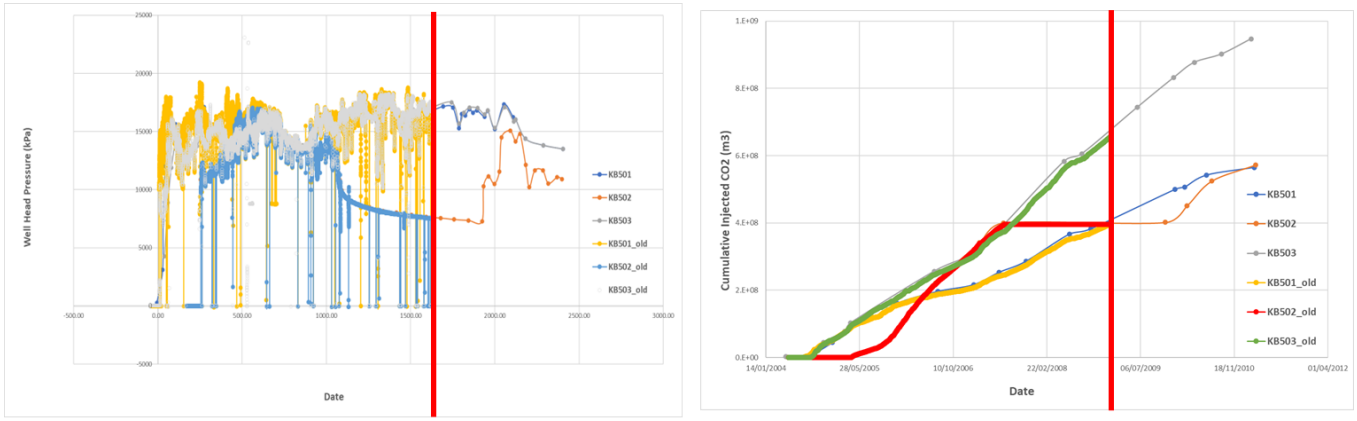

Figure 16 : WHP (left) and cumulative CO_2 injected volume (right) of injection wells over all the injection period. The red line denotes the end of the previous dataset.

Other minor changes in initial dataset regarding well operations are listed below:

- Reduce production rates when extrapolating data (to limit the impact on injection wells) in "*Block" version* datasets (see next section);
- Change relationship between BHP and WHP to be more relevant with other literature data.

New InSAR data coming for reprocessed satellite data were shared by SENSE partner (NGI) and aim to be compared with surface displacement calculations with the coupled hydromechanical simulations. InSAR data were then transformed for comparison with simulation results: we smoothed/upscaled the "raw" data (processed satellite data) to obtain collocated values as simulated ones with a gaussian filter (Figure 17). One of the advantages of this method is that it partly "denoises" the corresponding InSAR data.

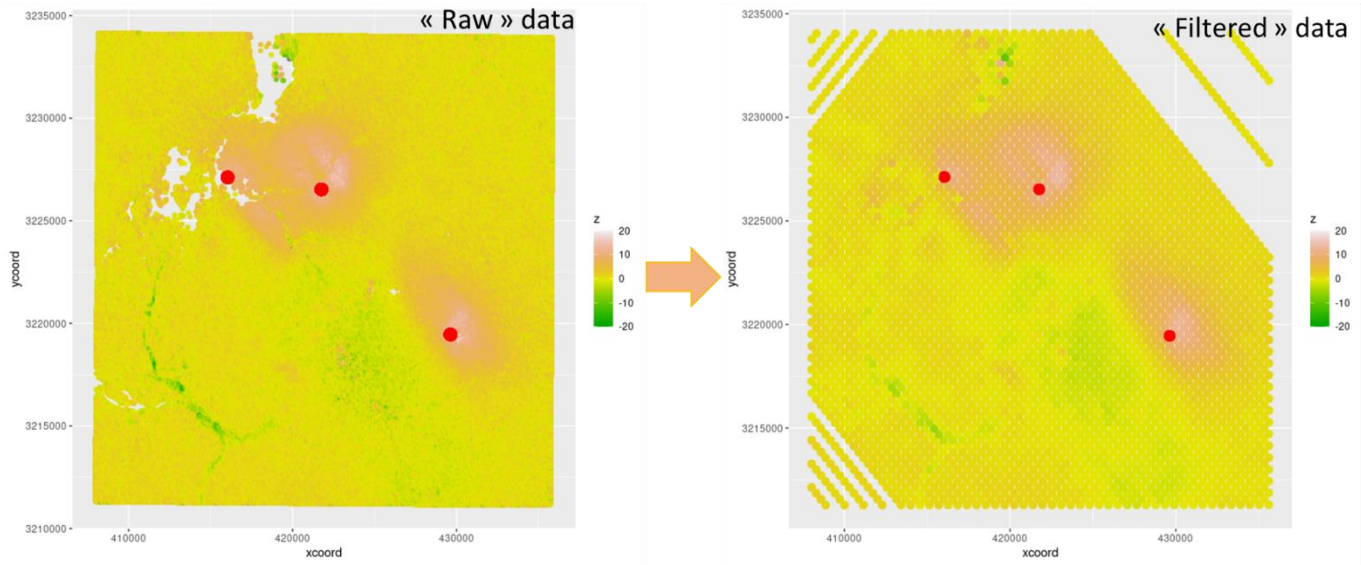

Figure 17 : Example of filtering and projection of InSAR data (left) to In Salah model spatial discretization via a gaussian filter (right). Red dots are injection wells head location.

To match all this new data, modifications will be applied on subsurface properties and are described in the next paragraphs.

Finally, to reduce the computational time of the coupled hydromechanical simulations, historical production and injection data were time-averaged, leading to a more reasonable number of considered time periods.

3.3 Trial of different underburden thicknesses

A first trial has been performed to study to dimension the underburden thickness for this problem. We consider two scenarios: one with a 500m-thick underburden and the second with a 4km-thick underburden.
An extreme case is studied with skeleton Young's moduli (varying with formation) in the order of dozens of GPa.
At the end of injection, the difference in surface displacement is locally at mm-scale (Figure 18, about 10% of difference). Cross-section of displacements in Z-direction (Figures 19 and 20) indicate that non-negligible displacements occurred deeper than the 500m-thick underburden. Consequently, models in the next section will have a 4km-thick underburden.

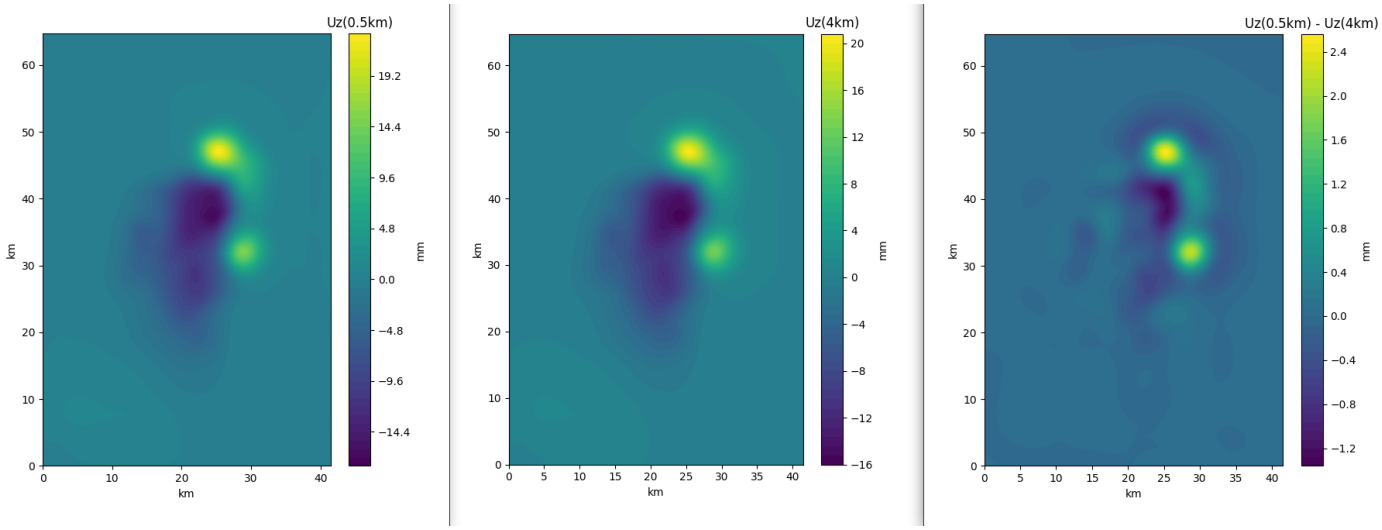

Figure 18 : Surface displacements for the 500m-thick underburden (left), the 4km-thick underburden (middle) and differences between both [in mm].

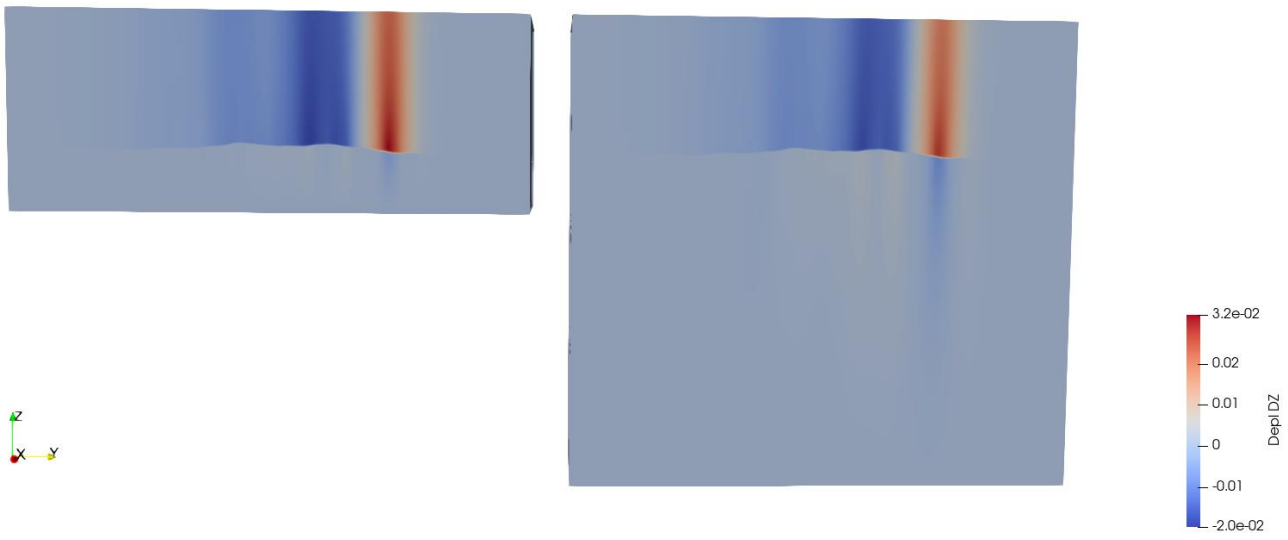

Figure 19 :Models' Cross-section. Comparison of displacement in Z-direction for different model's thickness (500m-thick underburden (left) and 4km-thick underburden).

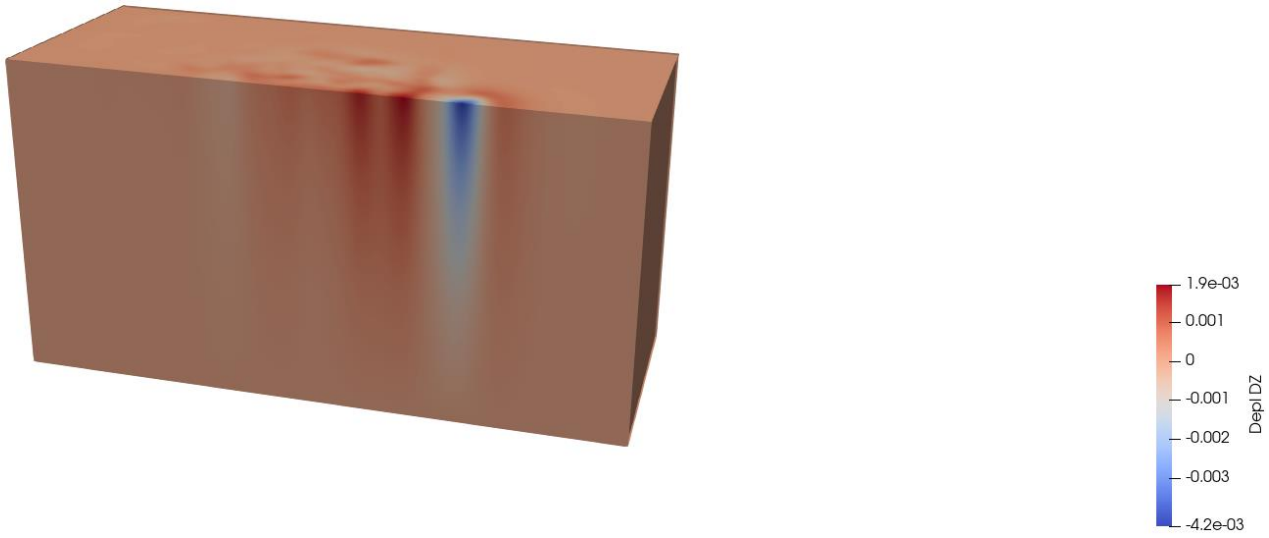

Figure 20 : Zoom in displacement in Z-direction below 500m of underburden for the model with a 4km-thick underburden.

4 In Salah model history-matching

The dual medium modelling is consistent with the characterization of the fractured medium description of In Salah. However, for calibration, it means that you can more than double the number of unknown parameters and consequently the degree of freedom, because of dual-medium parameters. This can render the inverse problem more difficult to solve.
To handle this problem, our first attempt was to separate flow and mechanical problems even though they are related to each other. This to gain computational time in a rather intensive-simulations process and to be able to reduce flow uncertain parameters and/or uncertainty ranges when handling the coupled problem.
Thus, we will first perform an history-matching on well pressure results then compare the resulting surface displacement with the InSAR data.

To do so, all our coupled simulations are calculated with the one-way configuration. We rely on flow simulator fracture pore compressibility as a dynamic parameter to make vary the fracture volume with pressure. Fracture compressibility values are relatively high ($10^{-8}Pa^{-1}$) that will imply a high increase in pore volume with pressure and partially reproduce a fracture reactivation when the increase in pressure is sufficiently high.
On the other hand, we should rely on dynamic permeability definition in flow simulator to change fracture flow properties when pressure goes beyond fracture pressure. We have to assign, per zone and/or formations, permeability multiplier values, for the fracture medium and for each direction, with corresponding absolute pressure values. To define the relationship between permeability multiplier M_i and pressure we rely on the Touhidi-Baghini expression (Touhidi-Baghini, 1998; Malinouskaya et al., 2018):

$$M_i(P,T) = \frac{K_i^{eff}}{K_i} = e^{\frac{\varepsilon_v C_i}{\varphi_0}}$$

Where i stands for x, y or z direction
C_i are material parameters to be defined
φ_0 is the initial porosity
ε_v is the volumetric strain when opening fractures (pressure P is above fracture pressure Po)
In the next section, temperature dependency is neglected (isothermal system), volumetric strain is defined such as:

$$\varepsilon_v = \varphi_0 C_p (P - P_o)$$

Where C_p stands for the pore compressibility
P_o is the pressure value for which permeability begins to increase, so here, the fracture pressure

Finally, it should be recalled that BHP values are calculated (internal tool) as a function of depth; flow rate, temperature and well head pressure and consequently are themselves uncertain (one can notice variations between different calculated BHPs from the literature).

4.1 Preliminary analysis

The aim of this preliminary study was to assess the impact on well results of additional changes in dual-medium permeability: either anisotropy or dynamic permeability change with pressure. In this first attempt, we consider the Krechba field as one block. For these cases, we are trying either to increase permeability ratio in Y-direction vs. X-direction, knowing that the Y-direction is the NW fracture orientation, described in previous section; or to increase permeability in Y and Z direction via dynamic permeability, since as described in the literature, fracture would have propagated preferentially in this NW direction and vertically.

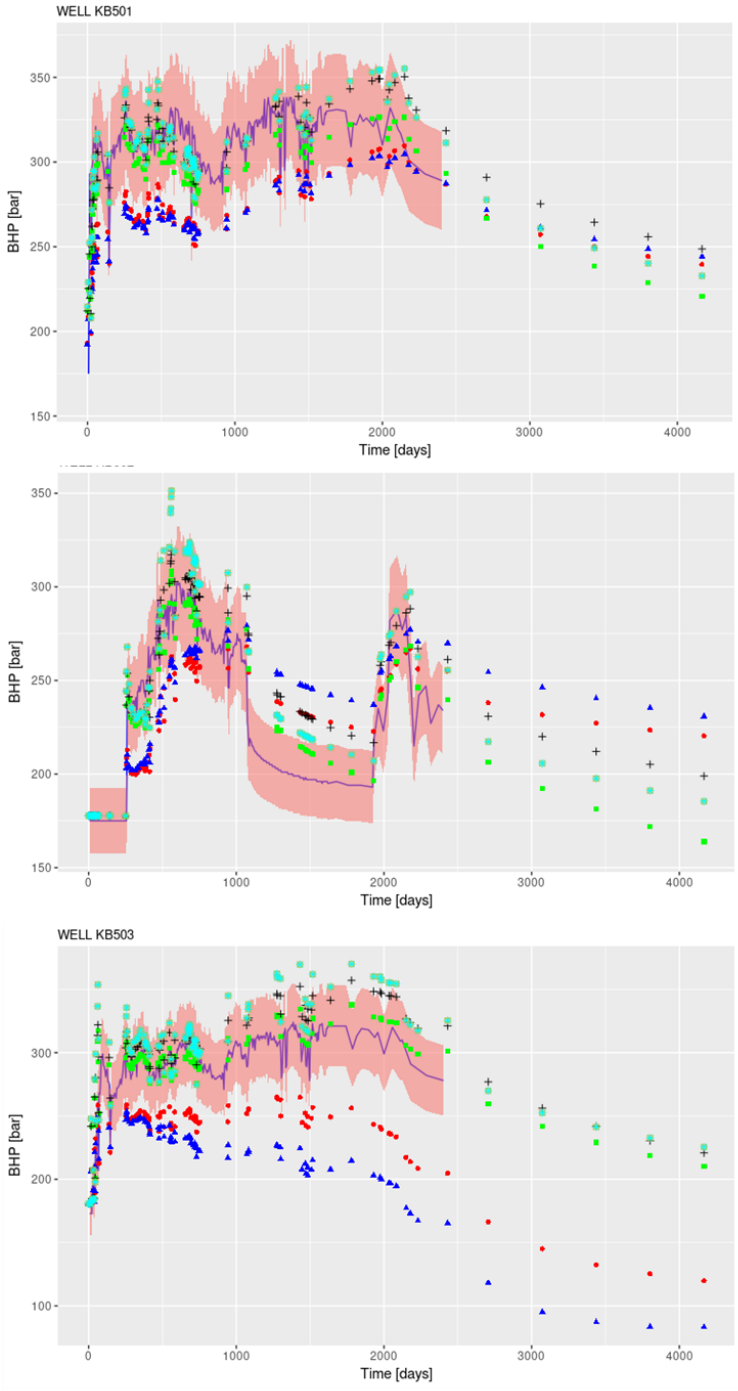

1. No additional anisotropy
   No dynamic permeability
2. Anisotropy in reservoir fracture zone: K_X*0.1 and K_Y*10
   No dynamic permeability
3. Anisotropy in reservoir fracture zone: K_X*0.1 and K_Y*10
   Dynamic permeability (K_Y & K_Z) in fracture zone
4. No additional anisotropy
   Dynamic permeability (K_Y & K_Z) in fracture zone
5. Anisotropy in reservoir fracture zone: Kx*0.5
   Dynamic permeability (K_Y & K_Z) in fracture zone

Figure 21 : Comparison of BHP results at KB501, KB502 and KB503 wells for different simulated scenarios (anisotropy and dynamic permeability). The purple line refers to field data with an uncertainty of +/- 10% (pink area). Light blue squares are results from the base case.

From Figure 21, it is clear that the base case overestimates the well BHPs, leading for some to reach the maximum overpressure and thus reducing the total injected volume. On the other hand, the attempt on anisotropy modifications (via permeability multiplier) reduces drastically the pressure to levels way below the measured values. If permeability values require to be modified to match data values, we have here at least some boundary values for the uncertainty range to be considered. Finally, the use of dynamic permeability seems to improve the match and allow to obtain a better simulation of the dynamic behavior at the wells.

In a second attempt, we compare results with or not a reduction in matrix and fracture compressibility (below one order of magnitude), with a change in production rates for the extrapolated ones (as discussed earlier) and with either a one-area model or a four areas model (as defined in Baroni et al., 2011): one area for the producers and one for each injection wells. Each area is defined with different permeability multipliers. For these cases, we do not consider dynamic permeability.

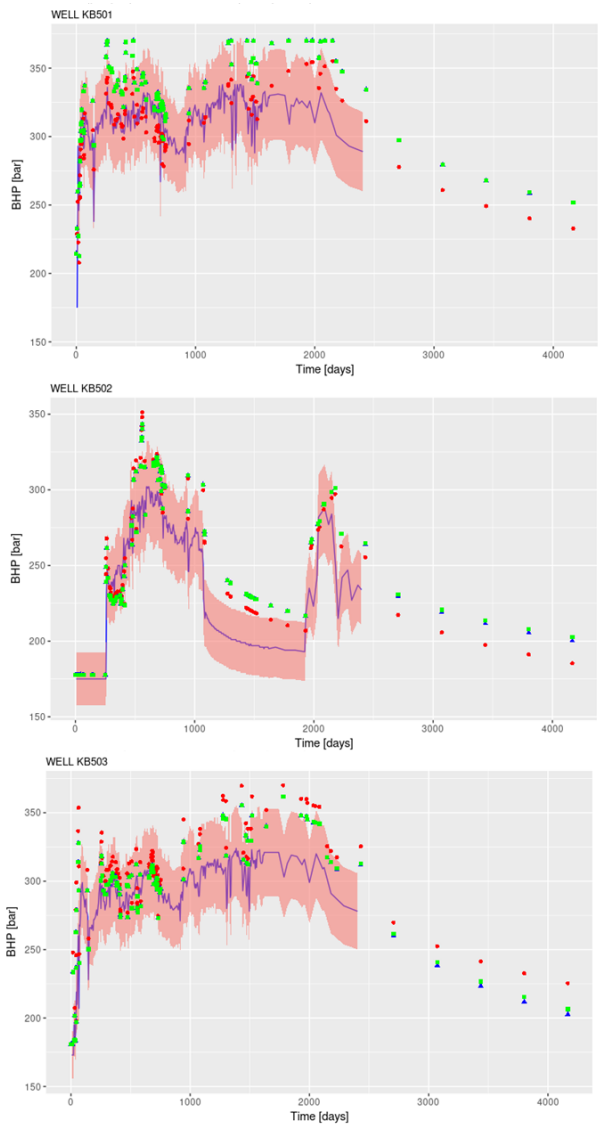

1. One block model - No additional anisotropy
   No dynamic permeability – One block model
2. Four blocks model - reduction of pore compressibility
   No dynamic permeability

	KB501	KB502	KB503
KX *	0.5	0.5	0.5
KY *	1	1.5	2

3. Four blocks model - reduction of pore compressibility
   No dynamic permeability
   Reduction of extrapolated production rates

	KB501	KB502	KB503
KX *	0.5	0.5	0.5
KY *	1	1.5	2

Figure 22 : Comparison of BHP results at KB501, KB502 and KB503 wells for different simulated scenarios (well blocks, pore compressibility and production rates). The purple line refers to field data with an uncertainty of +/- 10% (pink area). Red squares are results from the base case.

The suggested changes in permeability, this time without dynamic permeability, lead to an overestimate of BHP for KB501, while results are improved for KB503 and not significantly changed for KB502[2] (Figure 22).
The change in production rates in the latest periods do not impact much pressure results on injection wells. The impact of production wells on the injection ones seems to be limited.

[2] The pressure decline for KB502 is highly uncertain since the tool to convert WHP to BHP require a non-zero value for the injection rate. Here WHP are transformed to BHP by adding 130 bar to WHP values based on the only one calculating data with an injection rate value and corresponding WHP value in the decline period.

Based on these results, we will perform an assisted history-matching to find appropriate values for some of the uncertain parameters of this model.
In this next section, we will consider a model with four areas, since previous studies (Baroni et al., 2011 and Deflandre et al., 2011) have shown that a satisfactory history-matching for all wells could only be achieved by considering slightly different properties for the different well blocks. This has also been considered by others, for example Rinaldi et al. (2017) obtained different calibrated parameters values for each injection well.

4.2 Assisted sensitivity analysis and history-matching

We consider as uncertain, and thus to be calibrated the following parameters:

- Permeability Multiplier in X and Y-direction for the C10 formations, for matrix and fracture media and for each injector area (KB501, KB502, KB503)
- Pore Compressibility for the different formations (reservoir, caprock, overburden, underburden), for matrix and fracture media and for each injector area (KB501, KB502, KB503).

We could also have considered as uncertain the matrix block sizes of the dual medium definition and parameters of the dynamic permeability. However, as matrix block sizes have already been calibrated in a previous study and as they could be less influential parameters, we chose to keep the previous calibrated values. Moreover, in this first part of the history matching, we do not consider dynamic permeability to keep a reasonable number of uncertain parameters. Dynamic permeability will be used in a second step to adjust the calibrated model.
In fine, we have 32 uncertain parameters. Their uncertainty ranges are defined in table 5.

The calibration process aims to find parameters values such as to minimize the objective function, here the sum of square errors between simulated and measured data. To recall, measured data are the historical BHPs of the three injection wells and considering +/- 10% of measurement error.
Prior to the calibration, we perform a sensitivity analysis on the objective function to define the most contributing parameters to the objective function variations and, in fine, alleviate the inverse problem by considering only these selected parameters as to be calibrated.
To perform the sensitivity analysis and the optimization (for the calibration), we first calculate a surface response (also called metamodel or surrogate model) of the objective function. This because both sensitivity analysis and optimization are rather computational-intensive and cannot be achieved by dozens of thousands of flow simulator calls. Rather, we will calculate proxy-values of the objective function for both processes by using the metamodel which is a low-cost simulator (Feraille and Marrel, 2012). We build a metamodel of the objective function as a gaussian process and based on 250 flow simulations sampled following a Latin Hypercube Sampling (LHS) design of experiments. Q2 value for the objective function metamodel from a leave-one out cross-validation is 0.88, considered as satisfactory.

The sensitivity analysis is performed by calculating the Sobol indices (Sobol, 1993), representing the contribution of each parameter to the response variation. According to the results from the sensitivity analysis (Figure 23), the most contributing parameters are parameters from the fracture medium, namely, permeability-multipliers in X- and Y-direction and pore compressibility in storage formation. Thus, for the calibration, we only consider these parameters for all three wells to be calibrated. Other parameters are kept constant (median values).
For the optimization, i.e. minimization of the objective function, we applied gradient method on the surface response of the objective function. Because of potential local minima, the optimization process is repeated 200 times (with different initial points). Results are presented for the three wells in Figure 24. Results are not satisfactory in particular for KB501 and KB502.

Table 5: Uncertainty ranges for the considered model parameters. Cp stands for Pore Compressibiliy, main for matrix medium, Lcap for the Lower Caprock (C20), reserv for C10.2, reserv2 for C10.3, Ki for permeability multiplier in i-direction.

Variables	MIN	MAX
Cp_cap	1.00E-06	1.00E-05
Cp_und	5.00E-07	1.00E-05
Cpfis_Lcap_kb501	5.00E-04	0.01
Cpfis_Lcap_kb502	5.00E-04	0.01
Cpfis_Lcap_kb503	5.00E-04	0.01
Cpfis_reserv2_kb501	5.00E-04	0.01
Cpfis_reserv2_kb502	5.00E-04	0.01
Cpfis_reserv2_kb503	5.00E-04	0.01
Cpfis_reserv_kb501	5.00E-04	0.01
Cpfis_reserv_kb502	5.00E-04	0.01
Cpfis_reserv_kb503	5.00E-04	0.01
Cpmain_Lcap_kb501	1.00E-06	1.00E-05
Cpmain_Lcap_kb502	1.00E-06	1.00E-05
Cpmain_Lcap_kb503	1.00E-06	1.00E-05
Cpmain_reserv2_kb501	8.00E-07	8.00E-06
Cpmain_reserv2_kb502	8.00E-07	8.00E-06
Cpmain_reserv2_kb503	8.00E-07	8.00E-06
Cpmain_reserv_kb501	8.00E-07	8.00E-06
Cpmain_reserv_kb502	8.00E-07	8.00E-06
Cpmain_reserv_kb503	8.00E-07	8.00E-06
KxKB501	0.1	1.2
KxKB501main	0.1	1.2
KxKB502	0.1	1.2
KxKB502main	0.1	1.2
KxKB503	0.1	1.2
KxKB503main	0.1	1.2
KyKB501	0.5	10
KyKB501main	0.5	10
KyKB502	0.5	10
KyKB502main	0.5	10
KyKB503	0.5	10
KyKB503main	0.5	10

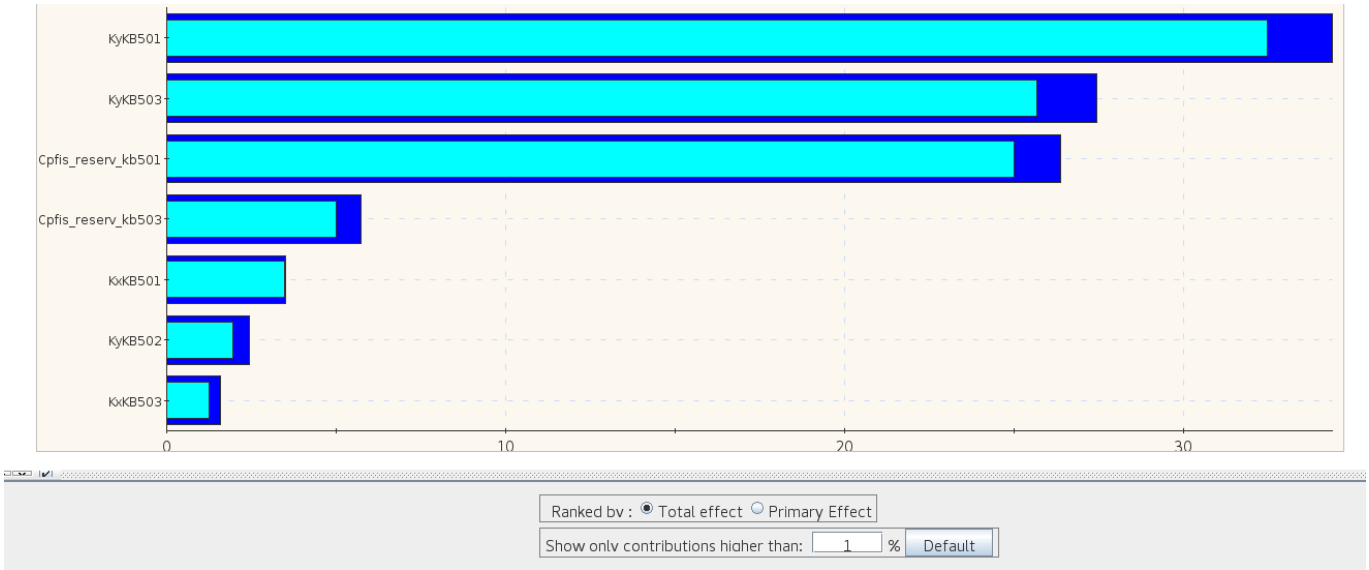

Figure 23 : Total Sobol' indices for the most contributing parameters to the surface response of the objective function considering all three injection wells.

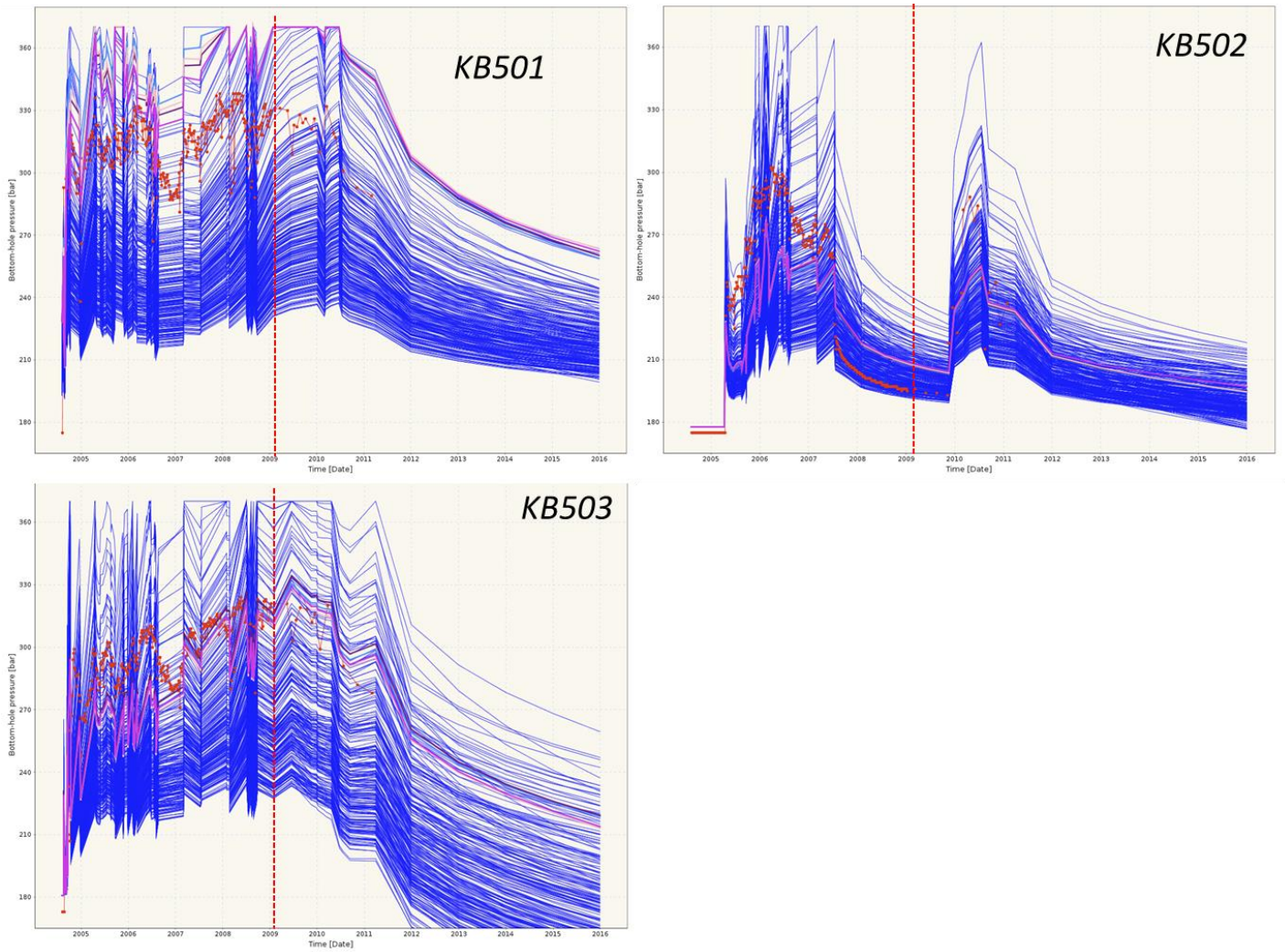

Figure 24 : BHP results from the initial 250 simulations (blue lines), measured data (red) and simulations with calibrated sensitive parameters (pink) from the optimization with the sum of wells objective functions. The vertical red dot lines represents the beginning of new measured data relatively to previous studies. Note that for matching KB502 data, we could have reduced the number of points in the decline period since, as said previously, it is the most uncertain period for the estimated BHP values

We adopt another calibration strategy to improve the history matching: we split the objective function into three with one objective function per well and we try to minimize each objective function independently. This should ease the optimization, assuming that properties from each well area does not much interfere with other well results. This is confirmed while building metamodels of the objective function for each well: according to the covariance coefficient values only sensitive parameters related to the studied well contribute significantly to the surface response variation. Thus, only parameters related to the studied well are used for the optimization process for each well. Q2 values for wells' metamodel from a leave-one out cross-validation is around 0.95 for KB501 and KB503, considered as satisfactory. Q2 for KB502 is low, around 0.7, and could have been improved by adding additional points in the design of experiments. Pressure results are presented in Figure 25, with simulation results combining optimized parameters for each well. Optimized parameters values are compared in Table 6. Results are significantly improved for KB-501 and slightly for KB502 and KB503. However, results are still inconsistent for KB501 at least at the end of the injection period.

Optimization may have been improved by improving metamodels of the objective function with more dedicated training data, i.e., building a new training sample with only optimized parameters as variables for metamodel calculation. As first line, this was disregarded due to the extra computational cost.

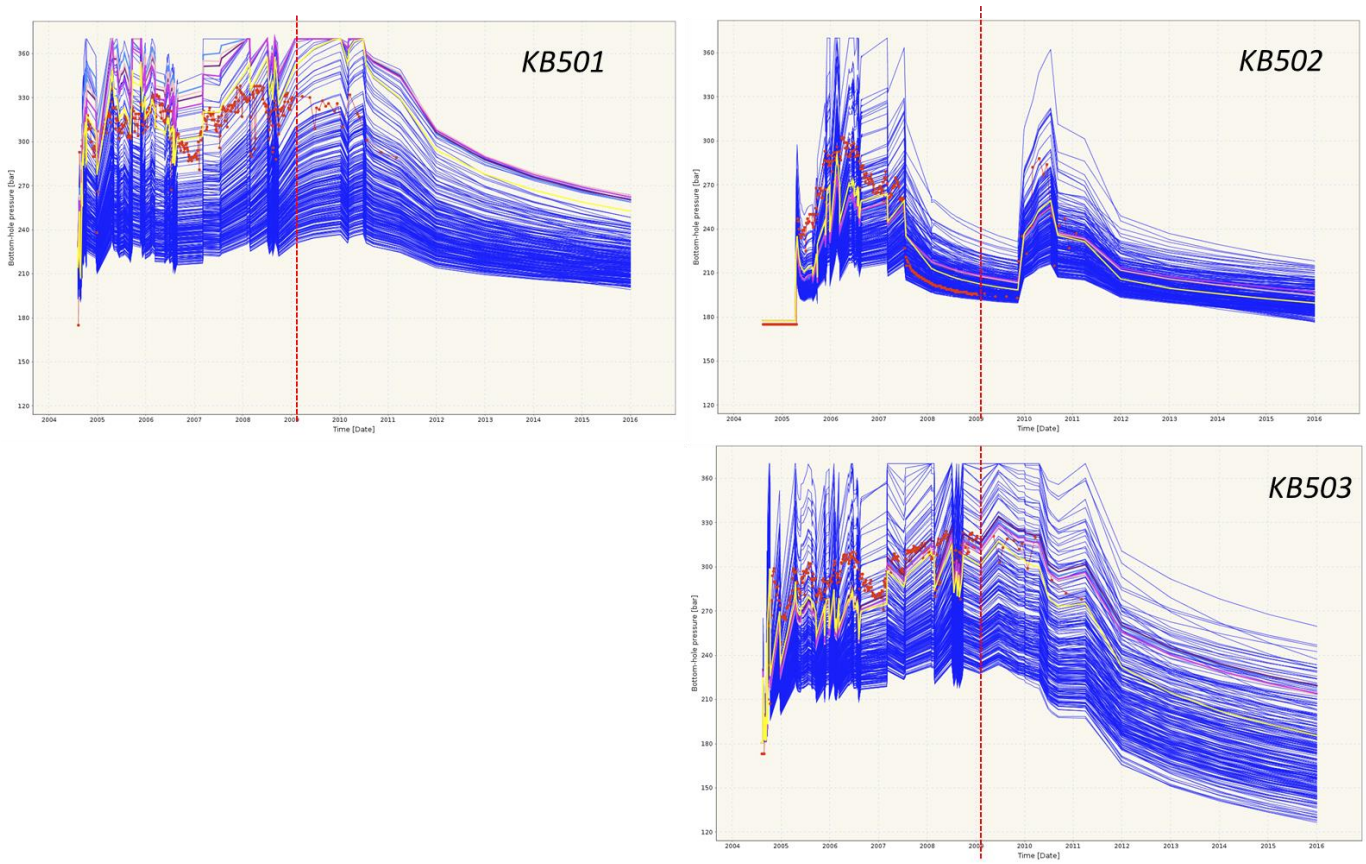

Figure 25 : BHP results from the initial 250 simulations (blue lines), measured data (red) and simulations with calibrated sensitive parameters from the optimization with the sum of wells objective functions (pink) and with independent wells objective functions (yellow). The vertical red dot lines represents the beginning of new measured data relatively to previous studies.

Table 6 : Optimized parameters' values function of the considered objective function (OF): either sum of wells errors (OF all Wells) or each well separately.

	OF all Wells	*OF KB501*	*OF KB502*	*OF KB503*
Cpfis_reserv_kb501 [bar^{-1}]	0.002	0.002	-	-
Cpfis_reserv_kb502 [bar^{-1}]	0.003	-	0.006	-
Cpfis_reserv_kb503 [bar^{-1}]	0.005	-	-	0.002
KxKB501 [-]	0.33	0.48	-	-
KxKB502 [-]	0.56	-	0.88	-
KxKB503 [-]	0.38	-	-	0.48
KyKB501 [-]	0.5	1.01	-	-
KyKB502 [-]	3.24	-	1.54	-
KyKB503 [-]	1.92	-	-	2.88

Thus, an additional strategy for the optimization is performed based on these previous results. We go back to the initial step of these processes with 32 uncertain parameters, but we modify the ranges of the previous influential parameters according to the last optimization results. Updated ranges for the uncertain parameters are in Table 7. A new batch of 250 simulations (LHS) is used as training sample.

Table 7 : Uncertainty ranges for the considered model parameters and modified following the previous optimization. Cp stands for Pore Compressibility, main for matrix medium, Lcap for the Lower Caprock (C20), reserv for C10.2, reserv2 for C10.3, Ki for permeability multiplier in i-direction.

Variables	MIN	MAX
Cp_und	5.00E-04	0.01
Cp_cap	5.00E-04	0.01
Cpfis_Lcap_kb501	5.00E-04	0.01
Cpfis_Lcap_kb502	5.00E-04	0.01
Cpfis_Lcap_kb503	5.00E-04	0.01
Cpfis_reserv2_kb501	5.00E-04	0.01
Cpfis_reserv2_kb502	5.00E-04	0.01
Cpfis_reserv2_kb503	5.00E-04	0.01
Cpfis_reserv_kb501	0.001	0.01
Cpfis_reserv_kb502	0.001	0.01
Cpfis_reserv_kb503	0.001	0.01
Cpmain_Lcap_kb501	1.00E-06	1.00E-05
Cpmain_Lcap_kb502	1.00E-06	1.00E-05
Cpmain_Lcap_kb503	1.00E-06	1.00E-05
Cpmain_reserv2_kb501	8.00E-07	8.00E-06
Cpmain_reserv2_kb502	8.00E-07	8.00E-06
Cpmain_reserv2_kb503	8.00E-07	8.00E-06
Cpmain_reserv_kb501	8.00E-07	8.00E-06
Cpmain_reserv_kb502	8.00E-07	8.00E-06
Cpmain_reserv_kb503	8.00E-07	8.00E-06
KxKB501	0.1	0.9
KxKB501main	0.1	1.2
KxKB502	0.1	0.9
KxKB502main	0.1	1.2
KxKB503	0.1	0.9
KxKB503main	0.1	1.2
KyKB501	0.5	5
KyKB501main	0.5	10
KyKB502	0.5	5
KyKB502main	0.5	10
KyKB503	0.5	5
KyKB503main	0.5	10

Even after this modification, the nine previous parameters remain the most influential, i.e., reservoir fracture parameters: permeability multipliers and pore compressibility. This time, a new training sample dedicated to these parameters is built for the objective function used in the optimization stage. 150 simulations (LHS) for these 9 parameters are sampled and 22 simulations are sampled (LHS) as validation sample. Two types of objective function are again considered:

1. Optimization of a unique objective function for all wells (i.e., sum of weighted square errors of all wells): **OF1**
2. Optimization of three objective functions simultaneously (i.e., differed from previous optimization attempt): one for each well (Multi-Objective): **OF2**

Q2 values from corresponding metamodels are:

- OF1: 0.84 with a leave-one out cross-validation on the training sample and 0.855 with the validation sample.
- OF2: 0.99, 0.71 and 0.98 with a leave-one out cross-validation on the training sample and 0.95, 0.94 and 0.99 with the validation sample resp. for KB501, KB502, KB503.

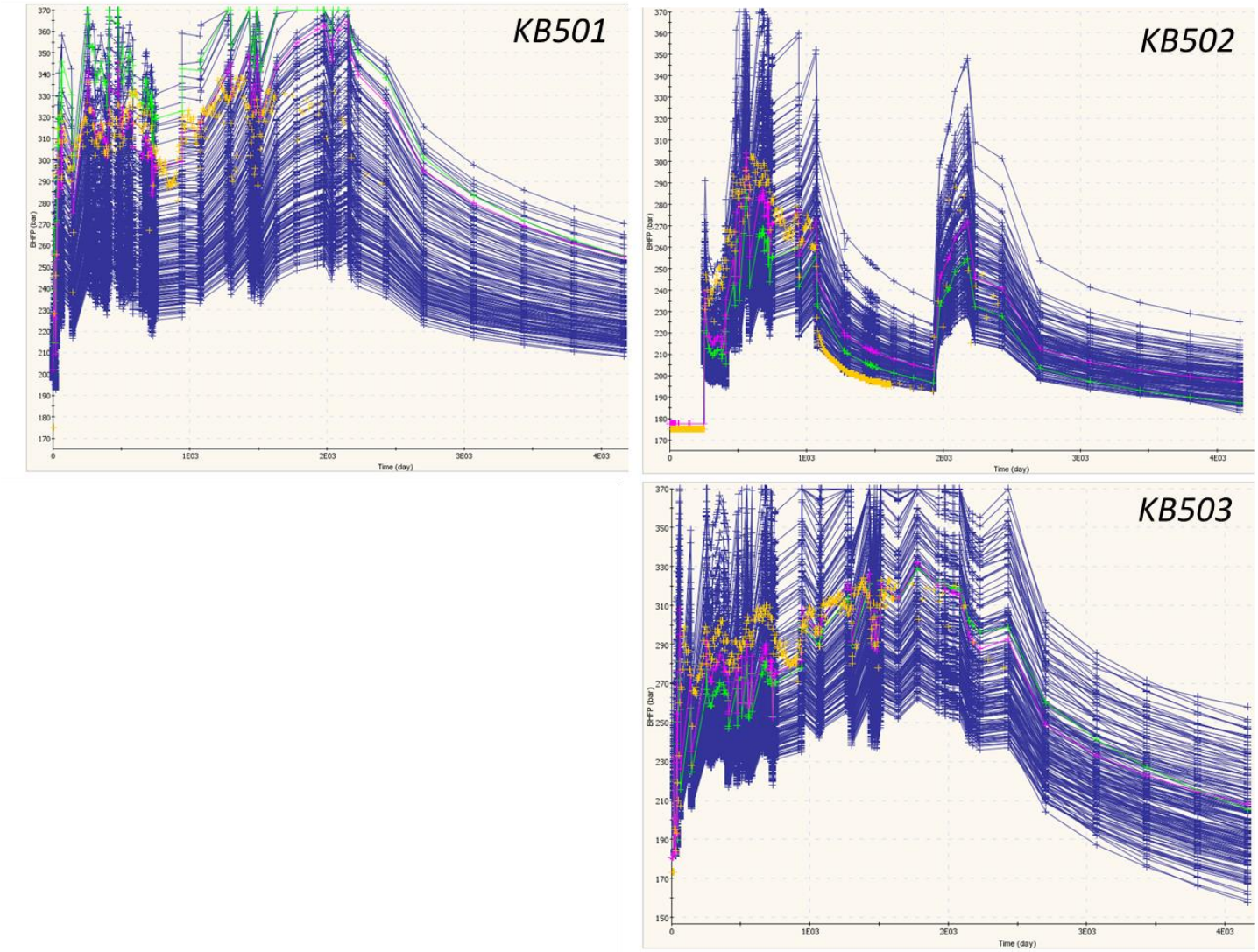

Figure 26 : BHP results from the training sample (150 simulations (blue lines)), measured data (yellow) and simulations with calibrated sensitive parameters from the optimization with OF1 (green) and with OF2 (pink).

The best matching is obtained with OF2 (multi-objective) with a significant improvement for KB501 and KB502 compared to previous optimizations (Figure 26). Calibrated parameters' values are summarized in Table 8.

Table 8 : Optimized parameters' values obtained with different objective functions: either the sum of wells errors (OF1) or the multi-objective one considering the OF for each well simultaneously (OF2).

	OF1: all Wells	*OF2: Multi OF*
Cpfis_reserv_kb501 [bar^{-1}]	0.001	0.001
Cpfis_reserv_kb502 [bar^{-1}]	0.006	0.006
Cpfis_reserv_kb503 [bar^{-1}]	0.004	0.03
KxKB501 [-]	0.467	0.246
KxKB502 [-]	0.9	0.596
KxKB503 [-]	0.1	0.627
KyKB501 [-]	0.984	2.623
KyKB502 [-]	1.725	1.264
KyKB503 [-]	2.924	1.765

In the following, we will use the optimized values from OF2 in our simulations, except for the pore compressibility of KB502: the optimized value is selected as minimizing the error over all the simulated period, however simulated pressure results at the beginning of the injection, before the hypothetical fracturing (around 285 MPa), are much lowered than measured ones. Consequently, we chose to reduce the KB502 pore compressibility to 4e-3 bar^{-1}, knowing that we will use dynamic permeability to take into account the enhanced permeability when reaching the pressure threshold.

Consequently, the last improvement in wells pressure history matching is by defining dynamic permeability as described in the beginning of this section. This time, calibration is performed by a trial-error procedure. We notice for some trials that changing parameters of dynamic permeability for one specific well does not impact pressure results for the other wells. This confirms a relatively low interference between injection wells. Pressure results with calibrated dynamic permeability functions are illustrated in Figure 27.

Consistent results were obtained for injection well pressure by defining a fracture pressure Po at 30 MPa for KB503, 29.5 MPa for KB501 and 28 MPa for KB502 for C10 formations and 0.5 MPa lower for the Lower Caprock. These fracture pressures are relevant with literature data, described in previous section. However, it appears that production wells behavior is not consistent with expected results: pressure decreases drastically and rapidly reaches the minimum pressure, stopping the production while CO_2 migrates quickly in the fracture medium reaching way earlier appraisal wells than expected. Indeed, we realize that no fluid flow from and to matrix medium: the dynamic permeability deactivates the dual medium configuration and only flow in fracture medium occurs. Thus, correction had to be made on flow simulator to prevent this effect. However, one can assume that pressure results at the injection wells are mainly controlled by fracture flow since pressure results were relevant compared to field data.

Updated results with correction on flow simulator are illustrated in Figures 28 with well pressure results and 29, 30 with pressure variations in fracture and matrix medium. With this correction, we obtain more consistent results in terms of fluid production and migration through fracture/matrix media: a significant amount of CO_2 reaches KB5 between August 2006 and March 2007. Some minor changes were applied on dynamic permeability since flow in matrix medium changes well injection results (see Table 9). Results illustrated the improvement brings with the dynamic permeability (Figure 28). But these results could be again improved to obtain a better history matching.

Table 9 : Parameters values used for the Touhidi-Bagigni expression for dynamic permeability

	KB501	**KB502**	**KB503**
Cy - *C20* [-]	9	8	6
Cz - *C20* [-]	11	10	8
Po - *C20* [MPa]	29	27.5	30.5
Cy - *C10.2; C10.3* [-]	50; 9	11; 8	10; 6
Cz - *C10.2; C10.3* [-]	60; 11	13; 20	13; 8
Po - *C10* [MPa]	29.5	28	31

One recommendation, about this historing-matching, would be to first calibrate static subsurface properties with only pressure results before the fracturing period. Then, based on this history-matching, continue the calibration with later pressure results for the dynamic permeability.
Notice also that dynamic permeability, as defined for the Lower caprock, was not sufficient to have a real impact since initial fracture permeability is very low (1e-10 m^2). Higher initial value and higher coefficient would be required for the Lower caprock to have a real impact and to emulate fracturing occurring in the Lower caprock. The same could apply for initial fracture porosity.

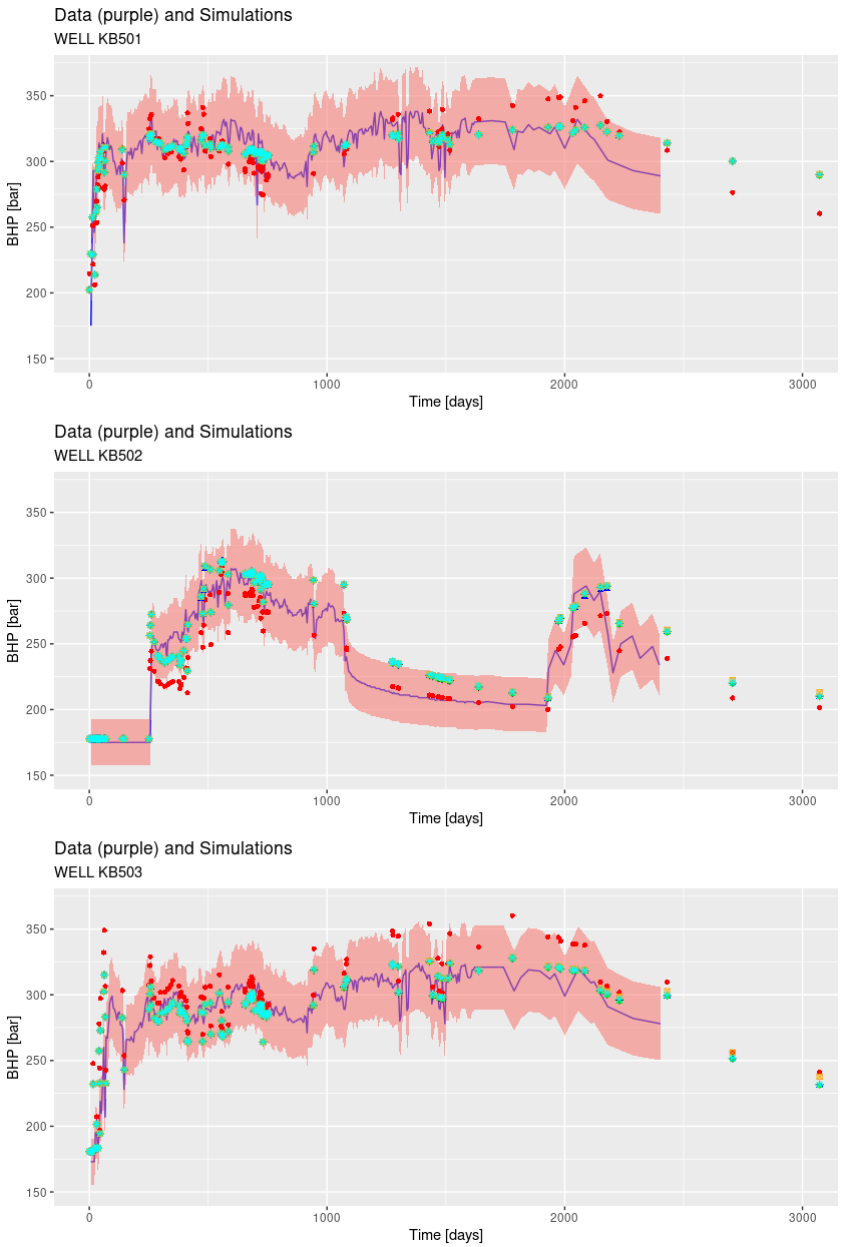

Figure 27 : BHP results from field data (purple with an uncertainty of +/- 10% (pink area)) and simulations with calibrated sensitive parameters from the first optimization (red, Cpfis_reserv_kb501 and Cpfis_reserv_kb503 = 2e-3 bar^{-1} and Cpfis_reserv_kb502 = 6e-3 bar^{-1} and permeability multipliers) and from the second optimization (OF2, Cpfis_reserv_kb501 and Cpfis_reserv_kb503 = 1e-3 bar^{-1} and Cpfis_reserv_kb502 = 4e-3 bar^{-1} and permeability multipliers) with dynamic permeability (green and yellow).

Figure 28 : BHP results from field data (purple with an uncertainty of +/- 10% (pink area)) and simulations with calibrated sensitive parameters from the second optimization (OF2, Cpfis_reserv_kb501 and Cpfis_reserv_kb503 = 1e-3 bar^{-1} and Cpfis_reserv_kb502 = 4e-3 bar^{-1} and permeability multipliers) with dynamic permeability (red), without dynamic permeability (blue) and with updated flow simulator and dynamic permeability (black and green).

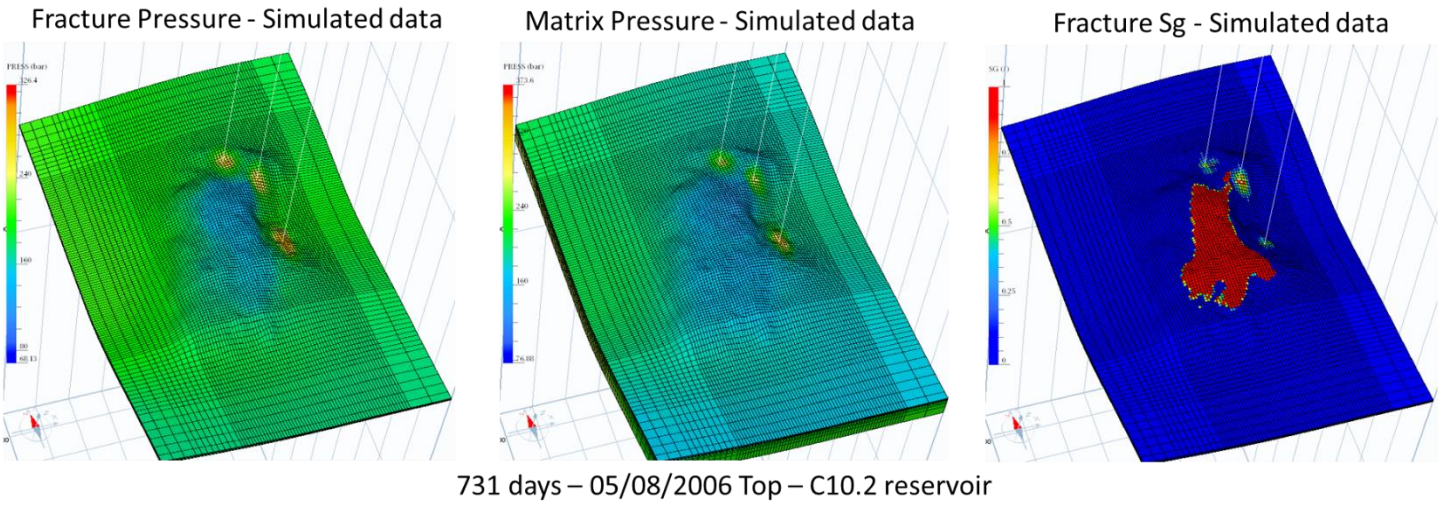

Figure 29 : Fracture and Matrix pressure, gas saturation in fracture medium after 731 days at the top of C10.2 formation.

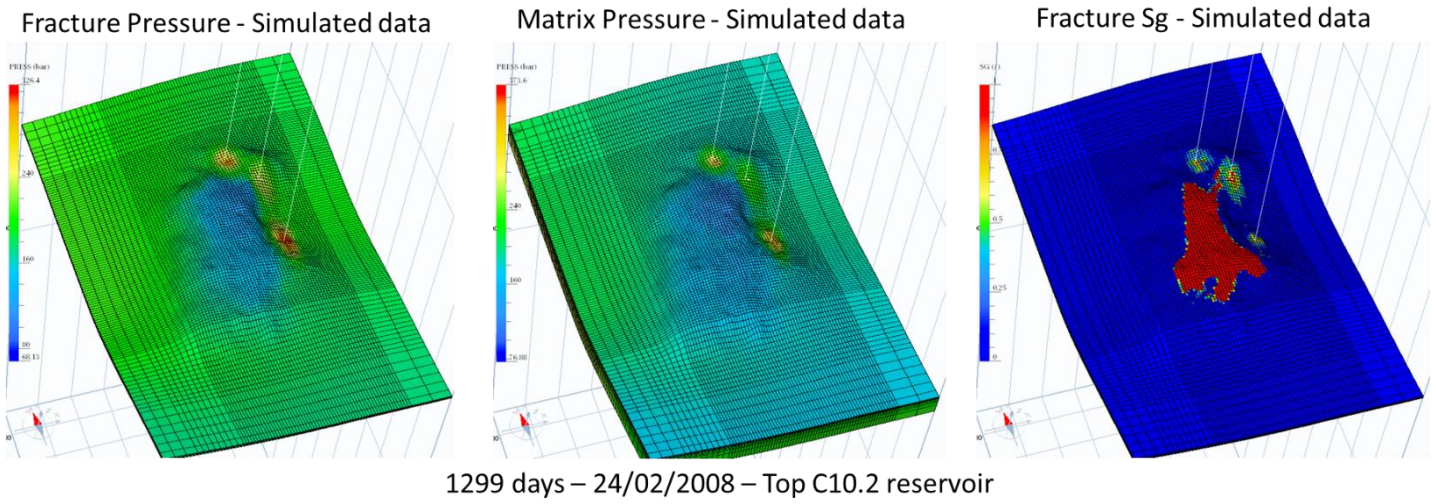

Figure 30 : Fracture and Matrix pressure, gas saturation in fracture medium after 1299 days at the top of C10.2 formation.

Finally, we compare surface displacements results from hydromechanical coupling simulations (one-way coupling) with InSAR data. Solid matrix elastic properties (Table 10) are defined such as homogenized values are relevant with literature data and corresponding pore compressibility values are close to the ones used in flow simulations for an averaged porosity value (Table 11). We recall that the homogenization results depend on uncertain parameters such as shape factor for fracture description but also on porosity values (varying laterally, on contrary to solid matrix properties defined by formation) and are highly sensitive to these values (see Deliverable 2.3).
Surface displacements results at the wells (Figure 31) are quite consistent for KB501 but are overestimated for KB503 and KB502. When looking at surface displacement maps, comparing simulations results and measured data (Figures 32 and 33), it is clear for KB503 that the misfit at the well is due to a preferential direction of surface displacement, not reproduced in the simulations: elongated pattern in KB503 area, related to the fracture orientation. For Kb-502, the double lobe-pattern is not reproduced in simulation, because no attempt was made to configure a high permeability zone in this area. Moreover, for KB-502, it seems that surface displacements mostly propagate to the North rather than towards KB-501, while for the simulation, the propagation around KB502 is quite symmetrical. This brings information on subsurface heterogeneities, on what is missing in the current modelling and ways to improve it.

Table 10 : Mechanical parameters values for hydromechanical coupling.

Depth range, m	Formation	Es [Pa]	vs [-]	Ehomog. [Pa]	vhomog. [-]
900-1650	Caprock	1.12E+10	0.33	9.15E+09	0.32
1650-1780	C20	8.6E+09	0.33	7.80E+09	0.3
1780-1800	C10.3	2.14E+10	0.32	1.50E+10	0.25
1800-1820	C10.2	6.29E+10	0.37	8.93E+09	0.13
1800-1820	C10.2 - KB 502	4.76E+10	0.4	6.88E+09	0.15
1800-1820	C10.2 - KB 503	6.04E+10	0.37	8.60E+09	0.13
1820-4000	Underburden (active flow cells)	1.88E+10	0.3	1.84E+10	0.3
0-900 / 1820-4000	Under/Over-burden (Inactive flow cells)	1.8E+10	0.29	7.70E+09	0.255

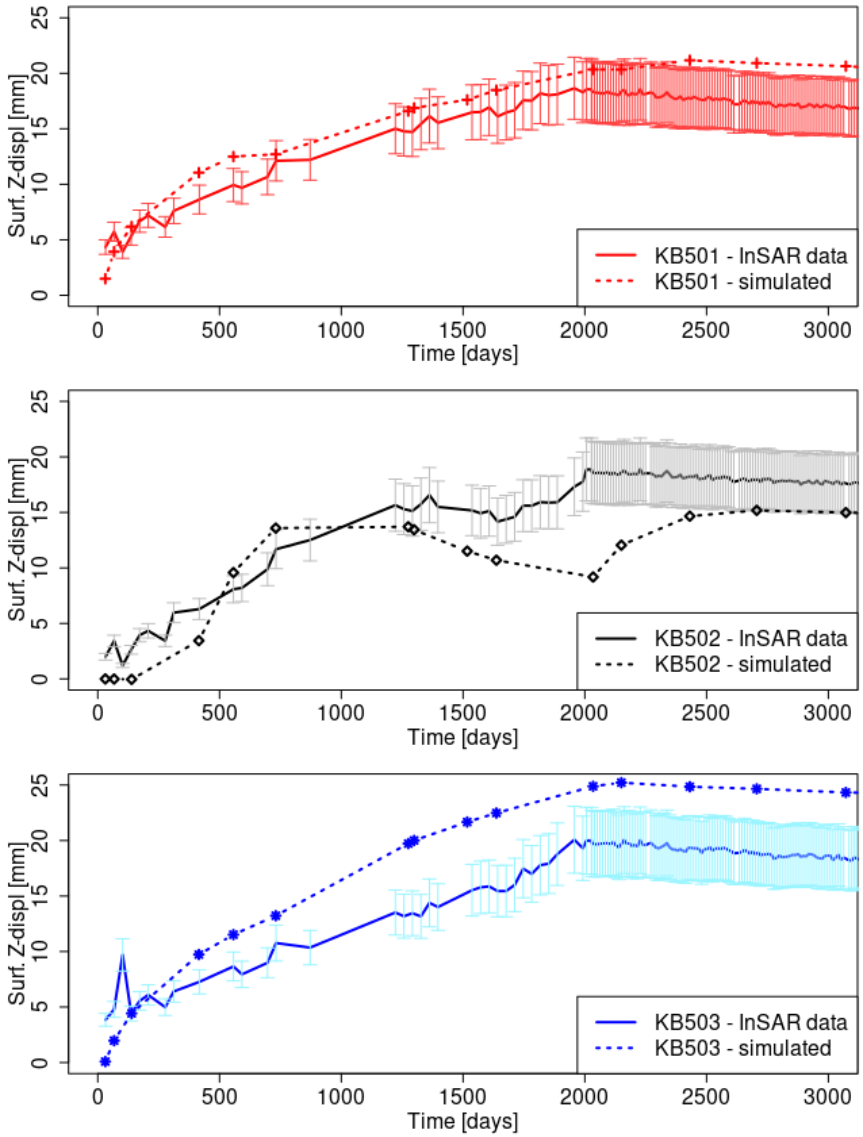

Figure 31 : Surface displacements in Z-direction for KB501, KB502 and KB503 wells function of time. Comparison between simulated data from the hydromechanical coupling and InSAR data (maximum displacements in wells area from filtered data, error bars of +/-15%).

The subsidence related to production is over-estimated in simulated results. Production data are not strictly representative of the field history so these results should be disregarded.

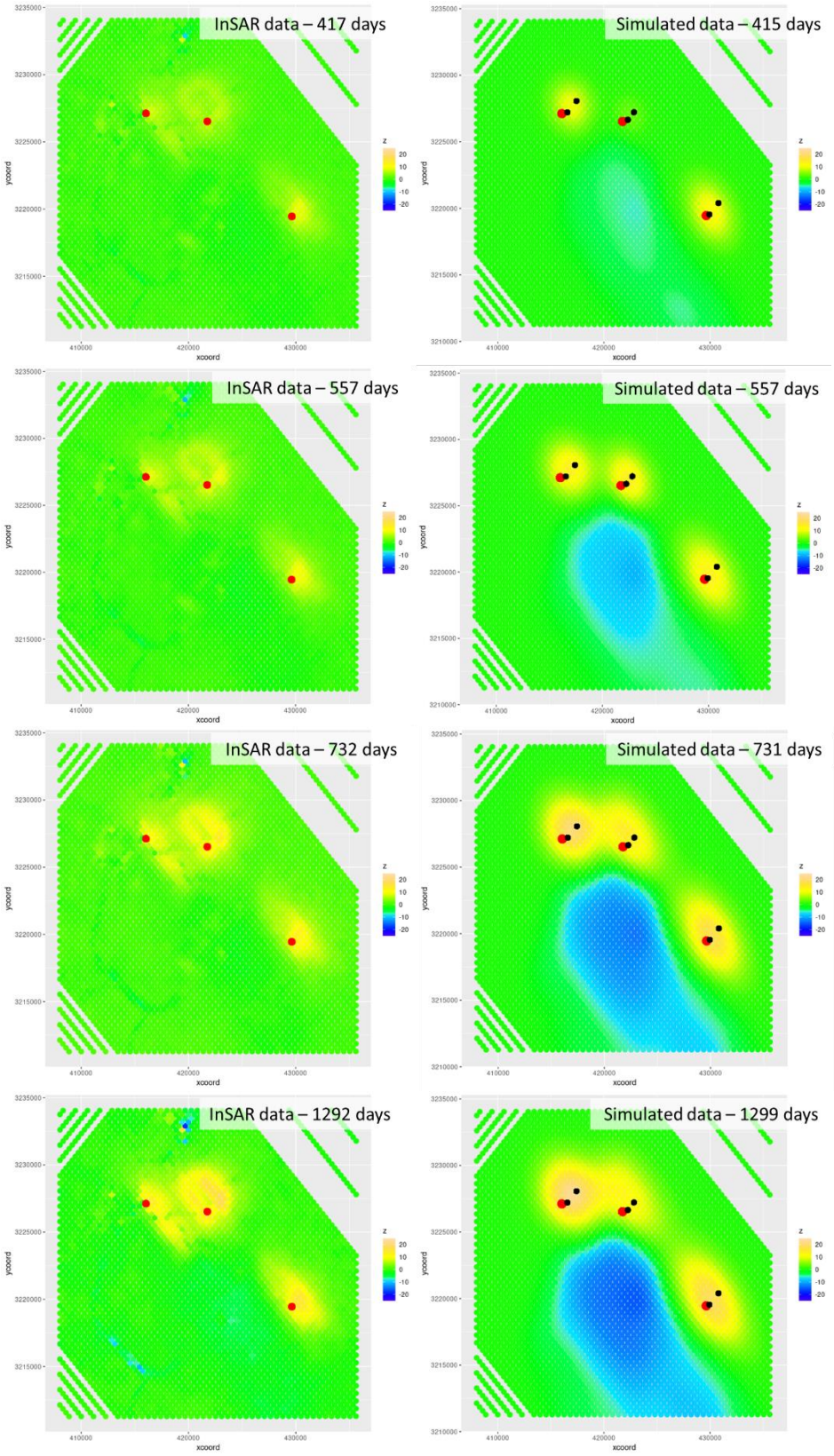

Figure 32 : Comparison of filtered InSAR data with simulated surface displacements maps. Because of the temporal discretization in periods for the hydromechanical coupling, dates are not always exactly the same between data and simulated ones (the closest are presented). Red dots are wells heads, black dots are heels and toes.

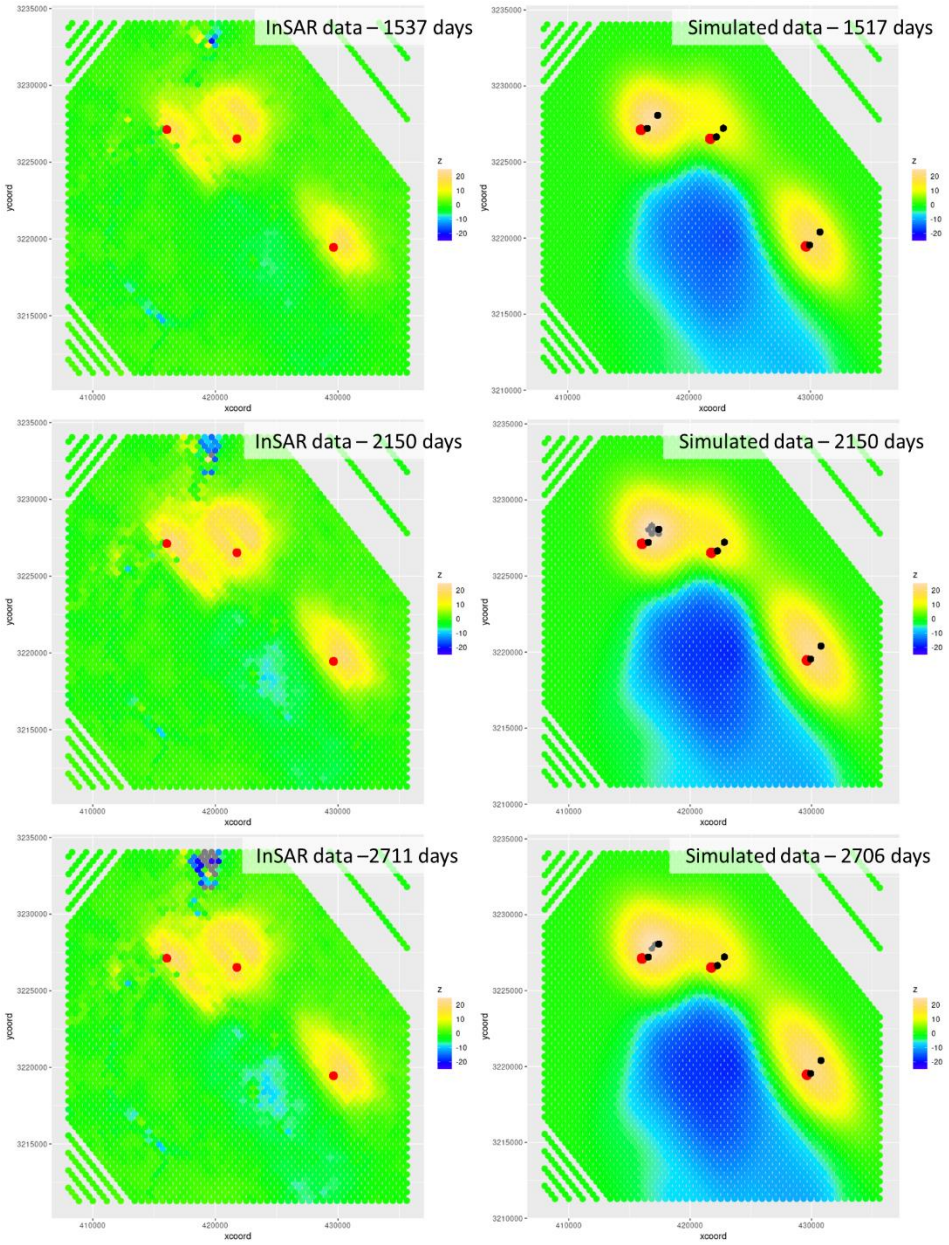

Figure 33 : [bis] Comparison of filtered InSAR data with simulated surface displacements maps. Because of the temporal discretization in periods for the hydromechanical coupling, dates are not always exactly the same between data and simulated ones (the closest are presented). Red dots are wells heads, black dots are heels and toes.

Table 11 : Pore compressibility values used in flow simulations and equivalent calculated from mechanical parameters values used in hydromechanical simulations.

Depth range, m	Formation	Cp_m flow [1/bar]	Cp_m flow [1/bar]	Cp_m eq mecha [1/bar]	Cp_f eq mecha flow [1/bar]
900-1650	Caprock	5.50E-06	-	2.00E-05	-
1650-1780	C20	5.50E-06	5.50E-03	2.50E-05	1.00E-02
1780-1800	C10.3	4.40E-06	5.25E-03	9.00E-06	4.80E-03
1800-1820	C10.2	4.40E-06	3.00E-03	4.20E-06	2.25E-03
1800-1820	C10.2 - KB 501	4.40E-06	1.00E-03	4.20E-06	2.25E-03
1800-1820	C10.2 - KB 502	4.40E-06	4.00E-03	5.60E-06	2.80E-03
1800-1820	C10.2 - KB 503	4.40E-06	3.00E-03	4.37E-06	2.30E-03
1820-4000	Underburden (active flow cells)	5.25E-06	-	1.00E-06	-
0-900 / 1820-4000	Under/Over-burden (Inactive flow cells)	5.25E-06	-	2.30E-06	-

5 Conclusions and Way Forward

An existing In Salah model has been updated regarding injection data and mechanical properties. This model has also been modified for compatibility with a newly developed hydromechanical coupling scheme for dual-medium. Modifications have been performed on this model to match injection well data and being consistent with production data and CO_2 breakthrough. With an assisted history-matching, combined with a sensitivity analysis, pore compressibility and permeabilities for the fracture medium have been adjusted. Fracture flow appears to be dominant in this case. A dynamic permeability setting has been required to obtain appropriate simulation results compared to field data. This is in agreement with previous studies (*e.g.*, Shi et al., 2012, Rinaldi et al., 2017, Bjornara et al., 2018). A comparison between simulated surface displacements and InSAR has been performed. While hydromechanical results are not irrelevant, more efforts are required to capture the heterogeneity in surface displacements related to a preferential orientation of fractures, faults, or damage zone (in particular for KB502 and KB 503).

Because injection wells do not seem to interfere much together and with production wells, in terms of pressure, one could have considered separate flow (or coupled hydromechanical) models for each injection wells as a first calibration trial. Results could then have been integrated in a full-field hydro-mechanical model, displacement being more diffuse than pressure footprint. We could have also realized the calibration with an additional step, considering a split in pressure data before and after fracture pressure is reached with a first history-match for the first period, before fracturing, with permeability values and pore compressibility (or elastic properties) calibration, then add dynamic permeability definition to match the period after fracturing.

More rigorously, the history-matching should have been applied to iterative coupled hydromechanical simulation results to adjust elastic properties (rather than pore compressibility) and to base the permeability evolution on mechanical volumetric deformation. But the problem complexity and the tool limitation have led to several simplifications.

To improve the calibration, and more specifically the representation of heterogeneities and their impact, one could consider using gradual and/or local deformation methods (Lu, 2000), leading to a better model representation, in particular for the surface displacement calibration. Additionally, local dissimilarity maps (LDM, Tillier et al., 2012) would be useful to add efficiently the comparison between InSAR and simulated surface displacement maps in the objective function.

Moreover, previous analyses demonstrate that thermal effects can have a significant impact on the displacement amplitude as for example in Bissel et al., 2011 and Rinaldi et al., 2018 for the specific case of In Salah field or more conceptually in Deliverable 2.3 (Bouquet et al., 2022). These thermal effects were neglected here but could be addressed in further studies.

Finally, the retroaction on permeability values related to the increase in fracture density could be implemented in the hydromechanical coupling scheme, rather than using ad-hoc dynamic permeability in flow simulation. This functionality is missing in the dual medium model but could improve hydromechanical simulation results (in the iterative coupling scheme) as it appears to be crucial for cases like In Salah, as it was underlined in this report.

6 Bibliography

Baroni, A., Estublier, E., Deflandre, J.-P., Daniel, J.-M., 2011. Modelling surface displacements associated with CO2 re-injection at Krechba. 45th US Rock Mechanics/Geomechanics Symposium.

Bissell, R.C., Vasco, D.W., Atbi, M., Hamdani, M., Okwelegbe, M., Goldwater, M.H., 2011. A full field simulation of the In Salah gas production and CO 2 storage project using a coupled geo-mechanical and thermal fluid flow simulator. Energy Procedia 4, 3290–3297 10th International Conference on Greenhouse Gas Control Technologies.

Bjornara, T.I., Bohli, B., Joonsang, P., 2018. Field-data analysis and hydromechanical modeling of CO2 storage at InSalah, Algeria, International Journal of Greenhouse gas control 79, 61-72

Bohloli, B., Bjornara, T.I., Bohli, B., Joonsang, P., Rucci, A., 2018. Can we use surface uplift data for reservoir performance monitoring? A case study from In Salah, Algeria. International Journal of Greenhouse Gas Control, Volume 76, Pages 200-207, ISSN 1750-5836, https://doi.org/10.1016/j.ijggc.2018.06.024.

Bouquet, S., Estublier, A., Fourno A., Frey J., Malinouskaya I., 2021. Assuring integrity of CO2 storage sites through ground surface monitoring (SENSE) - WP2.2: Understanding the mechanism of surface movement (Deliverable D2.2). SENSE report, Report D2.2, 89 p.

Bouquet, S., Bruch, A., Frey J., Cacas M.-C., 2022. Assuring integrity of CO2 storage sites through ground surface monitoring (SENSE) - WP2.3: Numerical simulation of ground movement in response to reservoir pressure change for the candidate sites (Deliverable D2.3). SENSE report, Report D2.3, 45 p.

Deflandre, J-P., Estublier, A., Baroni, A., Daniel, J-M., Adjémian, F., 2011. In Salah CO2 injection modeling: A preliminary approach to predict short term reservoir behavior. Energy Procedia, Volume 4, Pages 3574-3581, https://doi.org/10.1016/j.egypro.2011.02.286

Feraille, M., Marrel, A. (2012). Prediction under Uncertainty on a Mature Field. Oil & Gas Science and Technology – Rev. IFP Energies Nouvelles, Vol 67, No. 2, pp. 193-206. DOI: https://doi.org/10.2516/ogst/2011172.

Himri, Y., Malik, A., Stambouli, A., Himri, S., Belkacem, D., 2013. Review and use of the Algerian renewable energy for sustainable development. Renewable and Sustainable Energy Reviews. 13. 1584–1591. 10.1016/j.rser.2008.09.007.

Gibson-Poole, C.M., Raikes, S. Enhanced Understanding of CO2 storage at Krechba from 3D seismic. 9th annual conference on carbon capture and sequestration, Pittsburgh, Pennsylvania, May 10-13 (2010).

Iding, M., and Ringrose, P., 2010. Evaluating the impact of fractures on the performance of the In Salah CO2 storage site. International Journal of Greenhouse Gas Control, 4, 242-248, doi: 10.1016/j.ijggc.2009.10.016

Hu, L. Y. 2000 Gradual Deformation and Iterative Calibration of Gaussian-Related Stochastic Models. Mathematical Geology 32, 87–108.

Malinouskaya, I., Preux, C., Guy, N., Etienne, G., 2018. Impact of geomechanical effects during SAGD process in a meander belt. Oil & Gas Science and Technology - Revue d'IFP Energies nouvelles, 73, pp.17. ff10.2516/ogst/2018011.

Mathieson, A., Midgely, J., Wright, I., Saoula, N., Ringrose, P., 2011. In Salah CO2 Storage JIP: CO2 sequestration monitoring and verification technologies applied at Krechba, Algeria. Energy Procedia, Volume 4, Pages 3596-3603, ISSN 1876-6102, https://doi.org/10.1016/j.egypro.2011.02.289.

Morris, J.P., Haob, Y., Foxal, W., McNabb, W., "A study of injection-induced mechanical deformation at the In Salah CO2 storage project", International Journal of Greenhouse Gas Control, 5 (2011) 270–280

Rinaldi, A.P., Rutqvist, J., 2013. Modeling of deep fracture zone opening and transient ground surface uplift at KB-502 CO2 injection well, In Salah, Algeria. International Journal of Greenhouse Gas Control, 12 155–167.

Rinaldi, A.P., Rutqvist, J., Finsterle, S., Liu, H.-H., 2017. Inverse modeling of ground surface uplift and pressure with iTOUGH-PEST and TOUGH-FLAC: the case of CO2 injection at In Salah, Algeria. Comput. Geosci. 108, 98–109.

Ringrose, P. S., Atbi, M., Mason, D., Espinassous, M., Myhrer, O., Iding, M., Mathieson, 2009. Plume development around well KB-502 at the In Salah CO_2 storage site. First Break, volume 27.

Ringrose, P. S., Mathieson, A. S., Wright, I. W., Selama, F., Hansen, O., Bissell, R., and Midgley, J., 2013. The In Salah CO2 storage project: lessons learned and knowledge transfer, Energy Procedia, 37, 6226-6236.

Ringrose, Philip & Greenberg, Sallie & Whittaker, Steve & Nazarian, Bamshad & Oye, Volker. 2017. Building Confidence in CO2 Storage Using Reference Datasets from Demonstration Projects. Energy Procedia. 114. 3547–3557. 10.1016/j.egypro.2017.03.1484.

Rutqvist, J., Vasco, D.W., Myer, L., 2010. Coupled reservoir-geomechanical analysis of CO2 injection and ground deformations at In Salah, Algeria. International Journal of Greenhouse Gas Control, Volume 4, Issue 2, Pages 225-230, ISSN 1750-5836, https://doi.org/10.1016/j.ijggc.2009.10.017.

Shi, J.-Q., Sinayuc, C., Durucan, S., Korre, A., 2012. Assessment of carbon dioxide plume behaviour within the storage reservoir and the lower caprock around the KB-502 injection well at In Salah. Int. J. Greenh. Gas Control 7, 115–126.

Shi, J.-Q., Smith, J., Durucan, S., Korre, A., 2013. A coupled reservoir simulation-geomechanical modelling study of the CO 2 injection-induced ground surface uplift observed at Krechba, In Salah. Energy Procedia 37, 3719–3726.

Sobol, I.M, (1993). Sensitivity analysis for non-linear mathematical models, Mathematical modelling and computational experiment (translated from Russian: I.M. Sobol', sensitivity estimates for nonlinear mathematical models. Matematicheskoe Modelirovanie 2 (1990), 112–118 407–414).

Tillier E., Le Ravalec M., Da Veiga S. (2012) Simultaneous inversion of production data and seismic attributes: Application to a SAGD produced field, Oil Gas Sci. Technol. 67, 2, 289-301.

Touhidi-Baghini A. (1998) Absolute permeability of McMurray formation oil sands at low confining stress, PhD Thesis, Department of Civil and Environmental Engineering, Univ.of Alberta.

Vasco, D. W., A. Rucci, A. Ferretti, F. Novali, R. C., Bissell, P. S. Ringrose, A. S. Mathieson, and I. W. Wright, 2010. Satellite-based measurements of surface deformation reveal fluid flow associated with the geological storage of carbon dioxide. Geophys. Res. Lett., 37, L03303, doi:10.1029/2009GL041544.

Vasco, D.W., Bissell, R.C., Bohloli, B., Daley, T.M., Ferretti, A., Foxall, W., Goertz-Allmann, B.P., Korneev, V., Morris, J.P., Oye, V., Ramirez, A., Rinaldi, A.P., Rucci, A., Rutqvist, J., White, J. and Zhang, R. (2018). Monitoring

and Modeling Caprock Integrity at the In Salah Carbon Dioxide Storage Site, Algeria. In Geological Carbon Storage (eds S. Vialle, J. Ajo-Franklin and J.W. Carey). https://doi.org/10.1002/9781119118657.ch12

White, J., Chiaramonte, L., Ezzedine, S., Foxall, W., Hao, Y., Ramirez, A., McNab, W., 2013. Geomechanical behavior of the reservoir and caprock system at the In Salah CO2 storage project. Proceedings of the National Academy of Sciences, doi: 10.1073/pnas.1316465111.

Zhang, R., Vasco, D., Daley, T. M., and Harbert, W., 2015. Characterization of a fracture zone using attributes at the In Salah CO2 storage project, Interpretation, May, SM37-SM46, doi:10.1190/INT-2014-0141.1.

Annex A - Tables

1. Figures table

2. Tables table